



Delay-compensated control of sandwiched ODE–PDE–ODE hyperbolic systems for oil drilling and disaster relief[☆]

Ji Wang^{*}, Miroslav Krstic

Department of Mechanical and Aerospace Engineering, University of California, San Diego, La Jolla, CA 92093-0411, USA



ARTICLE INFO

Article history:

Received 13 October 2019

Received in revised form 1 June 2020

Accepted 9 June 2020

Available online 16 July 2020

Keywords:

Distributed parameter system

Delay

Boundary control

Oil drilling

Unmanned aerial vehicles

ABSTRACT

Motivated by engineering applications of subsea installation by deepwater construction vessels in oil drilling, and of aid delivery by unmanned aerial vehicles in disaster relief, we develop output-feedback boundary control of heterodirectional coupled hyperbolic PDEs sandwiched between two ODEs, where the measurement is the output state of one ODE and suffers a time delay. After rewriting the time-delay dynamics as a transport PDE of which the left boundary connects with the sandwiched system, a state observer is built to estimate the states of the overall system of ODE-heterodirectional coupled hyperbolic PDEs–ODE–transport PDE using the right boundary state of the last transport PDE. An observer-based output-feedback controller acting at the first ODE is designed to stabilize the overall system using backstepping transformations and frequency-domain designs. The exponential stability results of the closed-loop system, boundedness and exponential convergence of the control input are proved. The obtained theoretical result is applied to control of a deepwater oil drilling construction vessel as a simulation case, where the simulation results show the proposed control design reduces cable oscillations and places the oil drilling equipment to be installed in the target area on the sea floor. Performance deterioration under extreme and unmodeled disturbances is also illustrated.

© 2020 Elsevier Ltd. All rights reserved.

1. Introduction

1.1. Motivation

The first motivation of this work arises from off-shore oil drilling, where some equipment, such as a subsea manifold, a subsea pump station, a subsea distribution unit along with associated foundations, flowlines and umbilicals should be installed at designated locations (Standing, Mackenzie, & Snell, 2002; Stensgaard, White, & Schiffer, 2010) around the drill center on the seafloor. The installation of the equipment is completed by deepwater construction vessels (DCVs) (Stensgaard et al., 2010), because the installation sites are located outside a radius 45 m of the floating drilling platform (Fig. 2 in Stensgaard et al., 2010) and cannot be accessed by the huge floating drilling platform which has limited access and mobility (Stensgaard et al., 2010), and some of the equipment, such as flowlines, umbilicals, should be installed in advance to prepare to hook up the floating drilling platform when it arrives. The DCV is shown in Fig. 3, where the top of

the cable is attached to a crane on a vessel at the ocean surface and the bottom attached to equipment to be installed at the sea floor, referred to as payloads hereafter. The traditional method in underwater installation by DCVs is regulating the vessel dynamics position and manipulating the crane to obtain the desired heading for the payload (How, Ge, & Choo, 2010). It is not suitable for the deeper water construction in offshore oil drilling (more than a thousand meter) because the cable is very long when the payload is near the seabed, which would increase the natural period of the cable-payload system and introduce large oscillations (How et al., 2010; Wang, Koga, Pi and Krstic, 2018). The cable oscillations would cause large offset between the payload and the desired heading position of the crane, namely the designated installation location. In addition to large oscillations of the long cable, another challenge in the subsea installation is the existence of a sensor delay (How et al., 2010) which is due to the fact that the sensor signal is transmitted over a large distance from the seafloor to the vessel on the ocean surface through a set of acoustics devices (Ch. 10.6.6 in Sharma, 2017). It would result in information distortion or even make the control system lose stability. It is vital to design a delay-compensated control force at the onboard crane to reduce the cable oscillations and then place the equipment in the target area on the sea floor.

The second motivation is aid delivery to dangerous and inaccessible areas, such as flood, earthquake, fire, and industrial disaster victims via unmanned aerial vehicles (UAVs) (Guerrero,

[☆] The material in this paper was not presented at any conference. This paper was recommended for publication in revised form by Associate Editor Oswaldo Luiz V. Costa under the direction of Editor Richard Middleton.

* Corresponding author.

E-mail addresses: jiw248@eng.ucsd.edu (J. Wang), [\(M. Krstic\).](mailto:krstic@ucsd.edu)

Mercado, Lozano, & Garcia, 2015; Palunko, Cruz, & Fierro, 2012), where food, first-aid kits, referred to as suspended objects or payloads hereafter, are tied to the bottom of a cable, of which the other end is hanged to an UAV, i.e., a structure of UAV-cable-payload. The swing/oscillation of cable-payload would appear during the transportation motion due to the properties of the cable and external disturbances, such as wind, which may cause damage to the suspended object, the environment and the people around (Guerrero et al., 2015). At the end of the transport motion, when the UAV arrives at the location directly over to the rescue site and is ready to land the aid supplies, the suspended object naturally continues to swing (Palunko et al., 2012) which makes precisely placing these aid supplies at the target position difficult. Therefore, rapid suppression of oscillations of the cable and suspended object through a control force provided by rotor wings of the UAV is required. The measurement can be the oscillation acceleration of the suspended object by an accelerometer placed at the bottom end of the cable. Sensor delay would exist in the process of data acquisition, transmission and integration calculation to obtain the payload oscillation displacement which is used in constructing the observer and controller. In addition to aid delivery in disaster relief, UAV delivery is also used in some commercial cases to reduce labor cost. For example, some companies use UAVs to transport cargos in storehouses or lift and position building elements in architectural construction (Willmann et al., 2012). Some logistics companies have also begun to use UAVs to deliver packages in a small area (Guerrero et al., 2015).

The vibration/oscillation dynamics of cables are distributed parameter systems modeled by wave PDEs (He, He, Shi, & Sun, 2017; He, Meng, He, & Ge, 2018; Wang, Koga et al., 2018), and the crane/equipment and UAV/supplies at two ends of the cable can be regarded as lumped tip payloads described by ODEs (He & Ge, 2012, 2016). For the sake of order reduction, the wave PDEs with viscous damping terms describing the cable material damping can be converted to a class of heterodirectional coupled hyperbolic PDE systems (Anfinsen & Aamo, 2017; Deutscher, 2017a, 2017b; Deutscher, Gehring, & Kern, 2019) via Riemann transformations (Wang, Pi and Krstic, 2018). Therefore, the control problems in the aforementioned two applications come down to a theoretical problem about delay-compensated boundary control of a sandwiched coupled hyperbolic PDE system.

1.2. Control of PDE sandwiched system

Boundary control designs of a transport PDE sandwiched by two ODEs (Anfinsen & Aamo, 2018; Krstic, 2008, 2010a), viscous Burgers PDE (Liu & Krstic, 2000) or heat PDE (Wang & Krstic, 2019a) sandwiched systems were developed in the previous research. Control design of the coupled hyperbolic PDE sandwiched system mentioned in the last section is more challenging because of the in-domain instability which comes from in-domain couplings between PDEs. Recently, some results about state-feedback control of a coupled hyperbolic sandwiched system was proposed in Bou Saba, Bribiesca Argomed, Di Loreto, and Eberard (2017), Bou Saba, Bribiesca-Argomed, Loreto, and Eberard (2019) and Wang, Krstic and Pi (2018). Based on observer designs, output-feedback control of the coupled hyperbolic PDE sandwiched system was designed in Deutscher, Gehring, and Kern (2018) and Di Meglio, Lamare, and Aarsnes (2020). However, the aforementioned research has not investigated delay compensation (Bou Saba et al., 2019; Di Meglio et al., 2020) only achieve robustness to a small delay) in boundary control of sandwiched PDE systems. Actually, time-delay exists frequently in the practical engineering, especially the sensor delay, which exists in most practical sensor-used feedback systems. Considering time-delay compensation in the control design is an important step to apply theoretical results into practice.

1.3. Sensor delay compensation

The topic of sensor delay compensation has received much attention in the past three decades. In an advanced result presented in Krstic (2009) and Krstic and Smyshlyaev (2008), the sensor delay was captured as a transport PDE and then the original plant of ODE with sensor delay was rewritten as an ODE-transport PDE cascaded system without delay, before the observer/controller designs were conducted via backstepping. Therein, the observer was built as a “full-order” type which estimated both plant states and sensor states, compared with some classical results about sensor-delay-compensated observer designs (Ahmed-Ali, Karafyllis, & Lamnabhi-Lagarrigue, 2013; Cacace, Germani, & Manes, 2010; Germani, Manes, & Pepe, 2002) which only estimated plant states, namely “reduced-order” type. Using a model-based predictor, observer design for ODE systems with a time-varying sensor delay was presented in Krstic (2010b). Time-varying sensor delay compensation was also considered in Wang, Pi, Hu, and Zhu (2020) which designed a delay-compensated observer to estimate vibration states of a wave PDE modeled cable elevator. Boundary stabilization of a wave PDE whose boundary observation suffers a time delay was also proposed in Guo and Xu (2008). In the aforementioned work, the sensor delay was considered in the plant which is an ODE or a simple form PDE while the sensor delay in this paper exists in a more complex plant which is a sandwiched PDE system.

1.4. Main contribution

- Some restrictions on the proximal ODE structure in the previous results about boundary control of ODE-hyperbolic PDE-ODE sandwiched systems are relieved, such as the first-order and scalar form (Anfinsen & Aamo, 2018; Di Meglio et al., 2020), a chain of integrators (Wang, Krstic et al., 2018), $\det(C_0 B_0) \neq 0$ (Deutscher et al., 2018) and B_0 being invertible (Bou Saba et al., 2017).
- Compared with (Bou Saba et al., 2019) which first addressed the left invertible type proximal ODE in sandwiched PDEs, this paper further proposes observer-based output-feedback control design using a delayed measurement of which the delay length is constant and arbitrary. Compensation of sensor delay has not been investigated in control of sandwiched systems before. This is a more challenging task because the plant is extended to ODE-coupled hyperbolic PDEs-ODE-transport PDE after rewriting the delay as a transport PDE.
- The obtained theoretical result is applied to oscillation suppression of a DCV with compensating the sensor delay arising from large-distance transmission of the sensing signal via acoustics devices, where only one control force at the onboard crane is required while one more control force applied at the payload is required in How, Ge, and Choo (2011).

For complete clarity, the comparisons with the recent results of boundary control of sandwiched systems are summarized in Table 1.

1.5. Organization

The concerned model and the control task is described in Section 2. Observer design is proposed in Section 3. Therein, three transformations are used to convert the observer error system to a target observer error system whose exponential stability is straightforward to obtain, where all the dynamics output injections required in constructing the observer are determined.

Table 1

Comparisons with recent results of boundary control of linear ODE-PDE-ODE systems.

	Types of ODEs of actuation	Types of PDEs	Types of control systems	Delay compensation	Application to practical problems
Anfinsen and Aamo (2018)	First-order and scalar	Transport PDE	Output-feedback	×	×
Di Meglio et al. (2020)	First-order and scalar	2×2 coupled transport PDEs	Output-feedback	×	×
Wang, Krstic et al. (2018)	A chain of integrators	2×2 coupled transport PDEs	Output-feedback	×	×
Wang and Krstic (2019a)	A chain of integrators	Heat PDE	Output-feedback	×	×
Deutscher et al. (2018)	$\det(C_0 B_0) \neq 0$	n coupled transport PDEs	Output-feedback	×	×
Bou Saba et al. (2017)	B_0 being invertible	2×2 coupled transport PDEs	State-feedback	×	×
Bou Saba et al. (2019)	Left invertible	2×2 coupled transport PDEs	State-feedback	×	×
This paper	Left invertible	2×2 coupled transport PDEs	Output-feedback	✓	DCV

✓ denotes "included" and × denotes "not included".

Observer-based output-feedback control design is proposed in Section 4, where two transformations are applied to transform the observer to a so-called target system in a "stable-like" form except for the proximal ODE which is influenced by perturbations originating from PDEs and the distal ODE. After representing this target system in the frequency domain to obtain the relationships between the states of the proximal ODE and those perturbation states, the proximal ODE is reformulated as a new ODE without external perturbations in the frequency domain, and then the stabilizing control input is designed. The exponential stability of the closed-loop system and the boundedness and exponential convergence to zero of the control input are proved in Section 5. The obtained theoretical result is applied to oscillation suppression and position control of a DCV used for seabed installation as a simulation case in Section 6. The conclusions and a discussion of future work are provided in Section 7.

2. Problem formulation

2.1. Model description

The plant considered in this paper is

$$\dot{X}(t) = A_0 X(t) + E_0 w(0, t) + B_0 U(t), \quad (1)$$

$$z(0, t) = p w(0, t) + C_0 X(t), \quad (2)$$

$$z_t(x, t) = -q_1 z_x(x, t) - c_1 w(x, t) - c_1 z(x, t), \quad (3)$$

$$w_t(x, t) = q_2 w_x(x, t) - c_2 w(x, t) - c_2 z(x, t), \quad (4)$$

$$w(1, t) = q z(1, t) + C_1 Y(t), \quad (5)$$

$$\dot{Y}(t) = A_1 Y(t) + B_1 z(1, t), \quad (6)$$

$$y_{\text{out}}(t) = C_1 Y(t - \tau) \quad (7)$$

$\forall (x, t) \in [0, 1] \times [0, \infty)$. The block diagram of (1)–(7) is shown in Fig. 1. $X(t) \in \mathbb{R}^{n \times 1}$, $Y(t) \in \mathbb{R}^{m \times 1}$ are ODE states. $z(x, t) \in \mathbb{R}$, $w(x, t) \in \mathbb{R}$ are states of the 2×2 coupled hyperbolic PDEs with initial conditions $(z(x, 0), w(x, 0)) \in L^2(0, 1) \times L^2(0, 1)$. τ is an arbitrary constant denoting the time delay in the measurement. $U(t)$ is the control input to be designed. $c_1, c_2 \in \mathbb{R}$ and $E_0 \in \mathbb{R}^{n \times 1}$ are arbitrary. q_1 and q_2 are positive transport velocities. $q, p \in \mathbb{R}$ satisfy Assumption 1. $A_0 \in \mathbb{R}^{n \times n}$, $B_0 \in \mathbb{R}^{n \times 1}$, $C_0 \in \mathbb{R}^{1 \times n}$, $A_1 \in \mathbb{R}^{m \times m}$, $B_1 \in \mathbb{R}^{m \times 1}$, $C_1 \in \mathbb{R}^{1 \times m}$ satisfy Assumptions 2–3.

Assumption 1. p, q satisfy $|pq| < e^{\frac{c_2}{q_2} + \frac{c_1}{q_1}}$ and $q \neq 0$.

This assumption will be used in the output-feedback control design in Section 4.

Assumption 2. The pairs (A_0, B_0) , (A_1, B_1) are stabilizable and (A_0, C_0) , (A_1, C_1) are detectable.

According to Assumption 2, there exist constant matrices L_1, F_1, F_0 to make the following matrices Hurwitz:

$$\bar{A}_0 = A_0 - L_0 C_0, \quad (8)$$

$$\bar{A}_1 = A_1 - e^{\tau A_1} L_1 C_1 e^{-\tau A_1}, \quad (9)$$

$$\hat{A}_0 = A_0 - B_0 F_0, \quad (10)$$

$$\hat{A}_1 = A_1 - B_1 F_1. \quad (11)$$

Note that $A_1 - e^{\tau A_1} L_1 C_1 e^{-\tau A_1}$ has the same eigenvalues as $A_1 - L_1 C_1$ (Krstic & Smyshlyaev, 2008).

Assumption 3. (C_0, A_0, B_0) satisfy

$$\det \begin{pmatrix} sI - A_0 & B_0 \\ C_0 & 0 \end{pmatrix} \neq 0 \quad (12)$$

for all $s \in \mathbb{C}$, $\Re(s) \geq 0$.

Assumption 3 is about matrices of the proximal ODE- $X(t)$, namely actuator dynamics. Even though zeros in the closed right-half plane are excluded here while the zeros are allowed in some previous results on control of sandwiched PDE systems, such as (Deutscher et al., 2018), this assumption relieves some restrictions on the structure of the proximal ODE in the existing literature (such as A_0, B_0, C_0 being scalar in Anfinsen & Aamo, 2018; Di Meglio et al., 2020, B_0 being invertible in Bou Saba et al., 2017, $\det(C_0 B_0) \neq 0$ in Deutscher et al., 2018, or a form of a chain of integrators in Wang & Krstic, 2019a; Wang, Krstic et al., 2018) (Bou Saba et al., 2019). This assumption is equal to the existence of a stable left inversion system (Moylan, 1977) of (1) and is used in the control input design in Section 4.3.

Assumption 4. (C_1, A_1, B_1) satisfy

$$\det \begin{pmatrix} sI - A_1 & B_1 \\ C_1 e^{-\tau A_1} & 0 \end{pmatrix} \neq 0 \quad (13)$$

for all $s \in \mathbb{C}$, $\Re(s) \geq 0$.

Assumption 4 is about matrices of the distal ODE- $Y(t)$ with a sensor delay τ in the measurement output state. This assumption also prohibits the zeros of the ODE subsystem (C_1, A_1, B_1) are located in the closed right-half plane. It is not particularly restrictive and (C_1, A_1, B_1) is still quite general covering many application cases. This assumption is used in the observer design for the overall sandwiched system with the delayed measurement in Section 3. Note that if the sensor delay is zero, this assumption has the same form as Assumption 3.

Remark 1. The design in this paper also can be suitable for collocated control, namely the measurement is the output state of the proximal ODE $X(t)$ with a time delay τ , if (C_0, A_0, E_0) satisfies

$$\det \begin{pmatrix} sI - A_0 & E_0 \\ C_0 e^{-\tau A_0} & 0 \end{pmatrix} \neq 0$$

for all $s \in \mathbb{C}$, $\Re(s) \geq 0$.

The control objective of this paper: exponentially stabilize the overall sandwiched system, i.e., the ODE states $Y(t), X(t)$ and the PDE states $u(x, t), v(x, t)$, by constructing an output-feedback control input $U(t)$ applied at the proximal ODE $X(t)$, using the delayed measurement $y_{\text{out}}(t)$.

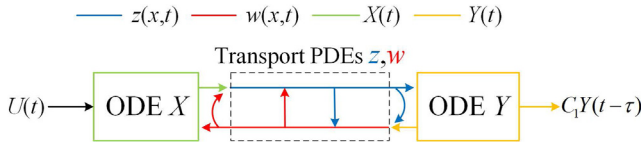


Fig. 1. Block diagram of the plant (1)–(7).

2.2. Rewrite delay as transport PDE

By defining

$$v(x, t) = C_1 Y(t - \tau(x - 1)), \quad \forall (x, t) \in [1, 2] \times [\tau, \infty) \quad (14)$$

we obtain a transport PDE

$$v(1, t) = C_1 Y(t), \quad (15)$$

$$v_t(x, t) = -\frac{1}{\tau} v_x(x, t), \quad (16)$$

$$y_{\text{out}}(t) = v(2, t) \quad (17)$$

$\forall (x, t) \in [1, 2] \times [\tau, \infty)$, to describe the time delay in the measurement (7). Replacing (7) by (15)–(17), we obtain a sandwiched hyperbolic PDE–ODE system connecting with another transport PDE, i.e., the following ODE–coupled hyperbolic PDEs–ODE–transport PDE system:

$$\dot{X}(t) = A_0 X(t) + E_0 w(0, t) + B_0 U(t), \quad (18)$$

$$z(0, t) = p w(0, t) + C_0 X(t), \quad (19)$$

$$z_t(x, t) = -q_1 z_x(x, t) - c_1 w(x, t) - c_1 z(x, t), \quad x \in [0, 1] \quad (20)$$

$$w_t(x, t) = q_2 w_x(x, t) - c_2 w(x, t) - c_2 z(x, t), \quad x \in [0, 1] \quad (21)$$

$$w(1, t) = qz(1, t) + C_1 Y(t), \quad (22)$$

$$\dot{Y}(t) = A_1 Y(t) + B_1 z(1, t), \quad (23)$$

$$v(1, t) = C_1 Y(t), \quad (24)$$

$$v_t(x, t) = -\frac{1}{\tau} v_x(x, t), \quad x \in [1, 2] \quad (25)$$

$$y_{\text{out}}(t) = v(2, t), \quad (26)$$

for $t \geq \tau$. Note that the time delay is “removed” at a cost of adding a transport PDE into the plant (1)–(7). Now, the control task is equivalent to exponentially stabilizing overall system (18)–(26), i.e., ODE(X)-PDE(z, w)-ODE(Y)-PDE(v), by constructing an output-feedback control input $U(t)$ at the first ODE (18), using the right boundary state of the last PDE (26).

3. Observer design

In order to build the observer-based output-feedback controller of the plant (1)–(7), in this section, we design a state-observer to track the overall system (1)–(7) only using the delayed measurement $y_{\text{out}}(t)$. Through the reformulation in Section 2.2, the estimation task is equivalent to designing a state-observer to recover the overall system (18)–(26) only using measurements at the right boundary $x = 2$ of the last transport PDE v .

The observer is built as a copy of the plant (18)–(26) plus some dynamics output injections:

$$\dot{\hat{X}}(t) = A_0 \hat{X}(t) + E_0 \hat{w}(0, t) + B_0 U(t) + h_1(y_{\text{out}}(t) - \hat{v}(2, t)), \quad (27)$$

$$\hat{z}(0, t) = p \hat{w}(0, t) + C_0 \hat{X}(t), \quad (28)$$

$$\hat{z}_t(x, t) = -q_1 \hat{z}_x(x, t) - c_1 \hat{w}(x, t) - c_1 \hat{z}(x, t) + h_2(y_{\text{out}}(t) - \hat{v}(2, t); x), \quad (29)$$

$$\hat{w}_t(x, t) = q_2 \hat{w}_x(x, t) - c_2 \hat{w}(x, t) - c_2 \hat{z}(x, t)$$

$$+ h_3(y_{\text{out}}(t) - \hat{v}(2, t); x), \quad (30)$$

$$\hat{w}(1, t) = q \hat{z}(1, t) + C_1 \hat{Y}(t) + h_4(y_{\text{out}}(t) - \hat{v}(2, t)), \quad (31)$$

$$\dot{\hat{Y}}(t) = A_1 \hat{Y}(t) + B_1 \hat{z}(1, t) + \Gamma_1(y_{\text{out}}(t) - \hat{v}(2, t)), \quad (32)$$

$$\hat{v}(1, t) = C_1 \hat{Y}(t), \quad (33)$$

$$\hat{v}_t(x, t) = -\frac{1}{\tau} \hat{v}_x(x, t) + h_5(y_{\text{out}}(t) - \hat{v}(2, t); x) \quad (34)$$

where a constant matrix Γ_1 and dynamics h_1, h_2, h_3, h_4, h_5 are to be determined. Initial conditions are taken as $(\hat{z}(x, 0), \hat{w}(x, 0), \hat{v}(x, 0)) \in L^2(0, 1) \times L^2(0, 1) \times L^2(1, 2)$. Defining observer error states as

$$\begin{aligned} & (\tilde{z}(x, t), \tilde{w}(x, t), \tilde{X}(t), \tilde{Y}(t), \tilde{v}(x, t)) \\ & = (z(x, t), w(x, t), X(t), Y(t), v(x, t)) \\ & \quad - (\hat{z}(x, t), \hat{w}(x, t), \hat{X}(t), \hat{Y}(t), \hat{v}(x, t)), \end{aligned} \quad (35)$$

according to (18)–(26) and (27)–(34), the observer error system is obtained as

$$\dot{\tilde{X}}(t) = A_0 \tilde{X}(t) + E_0 \tilde{w}(0, t) - h_1(\tilde{v}(2, t)), \quad (36)$$

$$\tilde{z}(0, t) = p \tilde{w}(0, t) + C_0 \tilde{X}(t), \quad (37)$$

$$\begin{aligned} \tilde{z}_t(x, t) & = -q_1 \tilde{z}_x(x, t) - c_1 \tilde{w}(x, t) - c_1 \tilde{z}(x, t) \\ & \quad - h_2(\tilde{v}(2, t); x), \end{aligned} \quad (38)$$

$$\begin{aligned} \tilde{w}_t(x, t) & = q_2 \tilde{w}_x(x, t) - c_2 \tilde{w}(x, t) - c_2 \tilde{z}(x, t) \\ & \quad - h_3(\tilde{v}(2, t); x), \end{aligned} \quad (39)$$

$$\tilde{v}(1, t) = q \tilde{z}(1, t) + C_1 \tilde{Y}(t) - h_4(\tilde{v}(2, t)), \quad (40)$$

$$\dot{\tilde{Y}}(t) = A_1 \tilde{Y}(t) + B_1 \tilde{z}(1, t) - \Gamma_1 \tilde{v}(2, t), \quad (41)$$

$$\tilde{v}(1, t) = C_1 \tilde{Y}(t), \quad (42)$$

$$\tilde{v}_t(x, t) = -\frac{1}{\tau} \tilde{v}_x(x, t) - h_5(\tilde{v}(2, t); x), \quad (43)$$

where $\Gamma_1 \tilde{v}(2, t)$ is an output injection, and $h_1(\tilde{v}(2, t)), h_2(\tilde{v}(2, t); x), h_3(\tilde{v}(2, t); x), h_4(\tilde{v}(2, t)), h_5(\tilde{v}(2, t); x)$ are dynamics output injections which are determined by

$$h_1(\tilde{v}(2, t)) = \mathcal{L}^{-1}[H_1(s)\tilde{v}(2, s)], \quad (44)$$

$$h_2(\tilde{v}(2, t); x) = \mathcal{L}^{-1}[H_2(s; x)\tilde{v}(2, s)], \quad (45)$$

$$h_3(\tilde{v}(2, t); x) = \mathcal{L}^{-1}[H_3(s; x)\tilde{v}(2, s)], \quad (46)$$

$$h_4(\tilde{v}(2, t)) = \mathcal{L}^{-1}[H_4(s)\tilde{v}(2, s)], \quad (47)$$

$$h_5(\tilde{v}(2, t); x) = \mathcal{L}^{-1}[H_5(s; x)\tilde{v}(2, s)], \quad (48)$$

where \mathcal{L}^{-1} denotes inverse Laplace transform and transfer functions $H_1(s), H_2(s; x), H_3(s; x), H_4(s), H_5(s; x)$ are to be determined later. Note that x in H_2, H_3, H_5 is only a parameter. Introducing (44)–(48) is helpful in constructing the dynamics $h_i(\cdot)$ in (27)–(34), because the algebraic relationships between $\tilde{v}(2, s)$ and other states can be obtained by using Laplace transform, and the transfer functions in (44)–(48) can be solved in algebraic equations after rewriting the required conditions of achieving an exponentially stable observer error system in the frequency domain.

Determination of $H_1(s), H_2(s; x), H_3(s; x), H_4(s), H_5(s; x)$ and Γ_1 in the observer (27)–(34), will be completed through the following three transformations which convert the observer error system (36)–(43) to a target observer error system whose exponential stability is straightforward to obtain.

3.1. First transformation

Applying the transformation:

$$\tilde{v}(x, t) = \tilde{\eta}(x, t) + \varphi(x)\tilde{Y}(t), \quad (49)$$

where $\varphi(x)$ is to be determined, we intend to convert (41)–(43) to a “stable-like” form as

$$\dot{\tilde{Y}}(t) = \bar{A}_1 \tilde{Y}(t) + B_1 \tilde{z}(1, t) - \Gamma_1 \tilde{\eta}(2, t), \quad (50)$$

$$\tilde{\eta}(1, t) = 0, \quad (51)$$

$$\tilde{\eta}_t(x, t) = -\frac{1}{\tau} \tilde{\eta}_x(x, t), \quad x \in [1, 2] \quad (52)$$

where \bar{A}_1 is a Hurwitz matrix defined in (9). In what follows, $\varphi(x)$, Γ_1 , $H_5(s; x)$ are determined in matching (41)–(43) and (50)–(52) via (49). Inserting the transformation (49) into (41), we have

$$\dot{\tilde{Y}}(t) = (A_1 - \Gamma_1 \varphi(2)) \tilde{Y}(t) + B_1 \tilde{z}(1, t) - \Gamma_1 \tilde{\eta}(2, t). \quad (53)$$

Considering (50), (9), Γ_1 should satisfy

$$\Gamma_1 \varphi(2) = e^{\tau A_1} L_1 C_1 e^{-\tau A_1}. \quad (54)$$

Evaluating (49) at $x = 1$ and applying (42), (51), we have

$$\tilde{v}(1, t) = \tilde{\eta}(1, t) + \varphi(1) \tilde{Y}(t) = \varphi(1) \tilde{Y}(t) = C_1 \tilde{Y}(t). \quad (55)$$

Therefore,

$$\varphi(1) = C_1. \quad (56)$$

Taking the time and spatial derivatives of (49) and submitting the result into (43), we have

$$\begin{aligned} & \tilde{v}_t(x, t) + \frac{1}{\tau} \tilde{v}_x(x, t) + h_5(\tilde{v}(2, t); x) \\ &= \tilde{\eta}_t(x, t) + \varphi(x) A_1 \tilde{Y}(t) + \varphi(x) B_1 \tilde{z}(1, t) - \varphi(x) \Gamma_1 \tilde{v}(2, t) \\ & \quad + \frac{1}{\tau} \tilde{\eta}_x(x, t) + \frac{1}{\tau} \varphi'(x) \tilde{Y}(t) + h_5(\tilde{v}(2, t); x) \\ &= \varphi(x) B_1 \tilde{z}(1, t) - \varphi(x) \Gamma_1 \tilde{v}(2, t) + h_5(\tilde{v}(2, t); x) \\ & \quad + \left[\varphi(x) A_1 + \frac{1}{\tau} \varphi'(x) \right] \tilde{Y}(t) = 0, \end{aligned} \quad (57)$$

where (41), (52) are used, and $\varphi(x)$ should satisfy

$$\varphi'(x) = -\tau A_1 \varphi(x), \quad (58)$$

to make $[\varphi(x) \bar{A}_1 + \frac{1}{\tau} \varphi'(x)] \tilde{Y}(t)$ zero, and $H_5(s; x)$ which determines $h_5(\tilde{v}(2, t); x)$ via (48) should be defined to ensure the rest term in (57) is zero, i.e.,

$$\varphi(x) B_1 \tilde{z}(1, t) - \varphi(x) \Gamma_1 \tilde{v}(2, t) + h_5(\tilde{v}(2, t); x) = 0. \quad (59)$$

Before determining $H_5(s; x)$, we solve conditions (54), (56), (58) to obtain $\varphi(x)$, Γ_1 as

$$\varphi(x) = C_1 e^{-\tau A_1(x-1)}, \quad x \in [1, 2] \quad (60)$$

$$\Gamma_1 = e^{\tau A_1} L_1. \quad (61)$$

Considering (51)–(52), we know

$$\tilde{\eta}(2, t) = 0, \quad t \geq \tau. \quad (62)$$

Thus (50) can be written as

$$\dot{\tilde{Y}}(t) = \bar{A}_1 \tilde{Y}(t) + B_1 \tilde{z}(1, t), \quad (63)$$

for $t \geq \tau$. Taking Laplace transform of (63), we have

$$(sI - \bar{A}_1) \tilde{Y}(s) = B_1 \tilde{z}(1, s), \quad (64)$$

where I is an identity matrix with appropriate dimension. Note: for brevity, we consider all zero initial conditions while taking Laplace transform (arbitrary initial conditions could be incorporated into the stability statement through an expanded analysis which is routine). Recalling \bar{A}_1 being Hurwitz, $\det(sI - \bar{A}_1)$ does not have any zeros in the closed right-half plane. Then the matrix

$sI - \bar{A}_1$ is invertible for any $s \in \mathbb{C}$, $\Re(s) \geq 0$. Multiplying both sides of (64) by $(sI - \bar{A}_1)^{-1}$, we have

$$\tilde{Y}(s) = (sI - \bar{A}_1)^{-1} B_1 \tilde{z}(1, s). \quad (65)$$

According to (49) and (62), we have

$$\tilde{v}(2, t) = \varphi(2) \tilde{Y}(t), \quad t \geq \tau. \quad (66)$$

Writing (66) in the frequency domain, inserting (60), (65) we have

$$\tilde{v}(2, s) = \varphi(2) \tilde{Y}(s) = r(s) \tilde{z}(1, s), \quad (67)$$

where

$$r(s) = C_1 e^{-\tau A_1} (sI - \bar{A}_1)^{-1} B_1. \quad (68)$$

Notice $r(s) \in \mathbb{R}$ due to $C_1 \in \mathbb{R}^{1 \times m}$ and $B_1 \in \mathbb{R}^{m \times 1}$.

Lemma 1. $r(s) = C_1 e^{-\tau A_1} (sI - \bar{A}_1)^{-1} B_1 \in \mathbb{R}$ is nonzero for any $s \in \mathbb{C}$, $\Re(s) \geq 0$ under Assumption 2 and 4.

Proof. Using (9) in Assumption 2, we have

$$\begin{aligned} & \begin{bmatrix} I & e^{\tau A_1} L_1 \\ 0 & I \end{bmatrix} \begin{bmatrix} sI - \bar{A}_1 & B_1 \\ C_1 e^{-\tau A_1} & 0 \end{bmatrix} \begin{bmatrix} I & -(sI - \bar{A}_1)^{-1} B_1 \\ 0 & I \end{bmatrix} \\ &= \begin{bmatrix} sI - \bar{A}_1 & 0 \\ C_1 e^{-\tau A_1} & -C_1 e^{-\tau A_1} (sI - \bar{A}_1)^{-1} B_1 \end{bmatrix}. \end{aligned} \quad (69)$$

Recalling Assumption 4, we know

$$\det \left(\begin{bmatrix} sI - \bar{A}_1 & 0 \\ C_1 e^{-\tau A_1} & -C_1 e^{-\tau A_1} (sI - \bar{A}_1)^{-1} B_1 \end{bmatrix} \right) \neq 0$$

for any $s \in \mathbb{C}$, $\Re(s) \geq 0$. Thereby $C_1 e^{-\tau A_1} (sI - \bar{A}_1)^{-1} B_1 \neq 0$. The proof of this lemma is completed. ■

According to Lemma 1, we know the existence of $r(s)^{-1} = \frac{1}{r(s)}$. Let us go back to (59) to determine $H_5(s; x)$ now. Taking Laplace transform of (59) and recalling (48), inserting (60) and (67), we have

$$\begin{aligned} & \varphi(x) B_1 \tilde{z}(1, s) - \varphi(x) \Gamma_1 \tilde{v}(2, s) + H_5(s; x) \tilde{v}(2, s) \\ &= \left[C_1 e^{-\tau A_1(x-1)} B_1 \right. \\ & \quad \left. - (C_1 e^{-\tau A_1(x-1)} \Gamma_1 - H_5(s; x)) r(s) \right] \tilde{z}(1, s) = 0. \end{aligned} \quad (70)$$

$H_5(s; x)$ is chosen as

$$\begin{aligned} H_5(s; x) &= C_1 e^{-\tau A_1(x-1)} \Gamma_1 - C_1 e^{-\tau A_1(x-1)} B_1 r(s)^{-1} \\ &= C_1 e^{-\tau A_1(x-1)} \Gamma_1 - \frac{C_1 e^{-\tau A_1(x-1)} B_1}{C_1 e^{-\tau A_1} (sI - \bar{A}_1)^{-1} B_1}, \end{aligned} \quad (71)$$

where Lemma 1 is used. Thereby, (70) holds. Then (59) holds by rewriting (70) in the time domain. Together with (58), then (57) holds for $t \geq \tau$. $h_5(\tilde{v}(2, t); x)$ can then be defined via (71) and (48). In the above, we have completed the conversion between (41)–(43) and (50)–(52) through (49) and determined Γ_1 , $h_5(\tilde{v}(2, t); x)$ needed in the observer. In what follows, $H_4(s)$ is determined to make the boundary condition (40) as zero, i.e.,

$$\tilde{w}(1, t) = q \tilde{z}(1, t) + C_1 \tilde{Y}(t) - h_4(\tilde{v}(2, t)) = 0. \quad (72)$$

Taking Laplace transform of (72) and recalling (47), inserting (65) and (67), we have

$$\begin{aligned} \tilde{w}(1, s) &= q \tilde{z}(1, s) + C_1 \tilde{Y}(s) - H_4(s) \tilde{v}(2, s) \\ &= (q + C_1 (sI - \bar{A}_1)^{-1} B_1 - H_4(s) r(s)) \tilde{z}(1, s) = 0. \end{aligned} \quad (73)$$

$H_4(s)$ is chosen as

$$H_4(s) = [q + C_1 (sI - \bar{A}_1)^{-1} B_1] r(s)^{-1}$$

$$= \frac{q + C_1(sI - \bar{A}_1)^{-1}B_1}{C_1 e^{-\tau A_1}(sI - \bar{A}_1)^{-1}B_1} \quad (74)$$

to make (73) hold. It follows that $\tilde{w}(1, t) = 0$ in (72) by rewriting $\tilde{w}(1, s) = 0$ in the time domain. $h_4(\tilde{v}(2, t))$ is thus determined by (47), (74). Therefore, through the first transformation (49) with determining the dynamics output injections $h_4(\tilde{v}(2, t))$, $h_5(\tilde{v}(2, t); x)$, (36)–(43) can be converted to the first intermediate system as

$$\dot{\tilde{X}}(t) = A_0 \tilde{X}(t) + E_0 \tilde{w}(0, t) - h_1(\tilde{v}(2, t)), \quad (75)$$

$$\tilde{z}(0, t) = p \tilde{w}(0, t) + C_0 \tilde{X}(t), \quad (76)$$

$$\begin{aligned} \tilde{z}_t(x, t) &= -q_1 \tilde{z}_x(x, t) - c_1 \tilde{w}(x, t) - c_1 \tilde{z}(x, t) \\ &\quad - h_2(\tilde{v}(2, t); x), \end{aligned} \quad (77)$$

$$\begin{aligned} \tilde{w}_t(x, t) &= q_2 \tilde{w}_x(x, t) - c_2 \tilde{w}(x, t) - c_2 \tilde{z}(x, t) \\ &\quad - h_3(\tilde{v}(2, t); x), \end{aligned} \quad (78)$$

$$\tilde{w}(1, t) = 0, \quad (79)$$

$$\dot{\tilde{Y}}(t) = \bar{A}_1 \tilde{Y}(t) + B_1 \tilde{z}(1, t), \quad (80)$$

$$\tilde{\eta}(1, t) = 0, \quad (81)$$

$$\tilde{\eta}_t(x, t) = -\frac{1}{\tau} \tilde{\eta}_x(x, t), \quad (82)$$

for $t \geq \tau$, where (79)–(82) are in a “stable-like” form while couplings, i.e., sources terms, exist in the domain $x \in [0, 1]$, i.e., (77)–(78). In the next subsection, we introduce the second transformation to decouple the couplings in (77)–(78).

3.2. Second transformation

We now apply the second transformation (Bin & Di Meglio, 2016)

$$\tilde{w}(x, t) = \tilde{\beta}(x, t) - \int_x^1 \psi(x, y) \tilde{\alpha}(y, t) dy, \quad (83)$$

$$\tilde{z}(x, t) = \tilde{\alpha}(x, t) - \int_x^1 \phi(x, y) \tilde{\alpha}(y, t) dy, \quad (84)$$

with the kernels $\psi(x, y), \phi(x, y)$ satisfying (86)–(89) in Wang and Krstic (2019b) ($K_1(y)$ in (87) of Wang & Krstic, 2019b and appearing in the following intermediate system will be defined in the next subsection where the well-posedness of $\psi(x, y), \phi(x, y)$ will be shown together with $K_1(y)$), to convert the first intermediate system (75)–(80) to the second intermediate system as

$$\begin{aligned} \dot{\tilde{X}}(t) &= A_0 \tilde{X}(t) + E_0 \tilde{\beta}(0, t) - E_0 \int_0^1 \psi(0, y) \tilde{\alpha}(y, t) dy \\ &\quad + h_1(\tilde{v}(2, t)), \end{aligned} \quad (85)$$

$$\tilde{\alpha}(0, t) = p \tilde{\beta}(0, t) + C_0 \tilde{X}(t) - \int_0^1 C_0 K_1(y) \tilde{\alpha}(y, t) dy, \quad (86)$$

$$\begin{aligned} \tilde{\alpha}_t(x, t) &= -q_1 \tilde{\alpha}_x(x, t) + \int_x^1 \bar{M}(x, y) \tilde{\beta}(y, t) dy \\ &\quad - c_1 \tilde{\alpha}(x, t) - c_1 \tilde{\beta}(x, t), \end{aligned} \quad (87)$$

$$\tilde{\beta}_t(x, t) = q_2 \tilde{\beta}_x(x, t) + \int_x^1 \bar{N}(x, y) \tilde{\beta}(y, t) dy - c_2 \tilde{\beta}(x, t), \quad (88)$$

$$\tilde{\beta}(1, t) = 0, \quad (89)$$

$$\dot{\tilde{Y}}(t) = \bar{A}_1 \tilde{Y}(t) + B_1 \tilde{\alpha}(1, t), \quad (90)$$

for $t \geq \tau$, with defining

$$\bar{M}(x, y) = \int_x^y \phi(x, \delta) \bar{M}(\delta, y) d\delta - c_1 \phi(x, y), \quad (91)$$

$$\bar{N}(x, y) = \int_x^y \psi(x, \delta) \bar{M}(\delta, y) d\delta - c_1 \psi(x, y). \quad (92)$$

Note that $\tilde{\eta}(\cdot, t)$ (81)–(82) is removed for brevity because $\tilde{\eta}(\cdot, t) \equiv 0, t \geq \tau$. In what follows, $H_2(s; x), H_3(s; x)$ are determined in matching the first intermediate system (75)–(80) and the second intermediate system (85)–(90) via (83)–(84). Inserting (83)–(84) into (78) along (87)–(88), and applying (86)–(88) in Wang and Krstic (2019b), (92), we have

$$\begin{aligned} \tilde{w}(x, t) &- q_2 \tilde{w}_x(x, t) + c_2 \tilde{z}(x, t) + c_2 \tilde{w}(x, t) + h_3(\tilde{v}(2, t); x) \\ &= q_1 \psi(x, 1) \tilde{\alpha}(1, t) + h_3(\tilde{v}(2, t); x) = 0, \end{aligned} \quad (93)$$

of which the detailed calculation is shown in (B.1) in Wang and Krstic (2019b). We thus know the following equation should be satisfied

$$q_1 \psi(x, 1) \tilde{\alpha}(1, t) + h_3(\tilde{v}(2, t); x) = 0, \quad (94)$$

where $\tilde{\alpha}(1, t) = \tilde{z}(1, t)$ according to (84) is used. Writing (94) in the frequency domain and applying (46), (67), we have

$$\begin{aligned} q_1 \psi(x, 1) \tilde{z}(1, s) + H_3(s; x) \tilde{v}(2, s) \\ = (q_1 \psi(x, 1) + H_3(s; x) r(s)) \tilde{z}(1, s) = 0. \end{aligned} \quad (95)$$

$H_3(s; x)$ should be chosen as

$$H_3(s; x) = -q_1 \psi(x, 1) r(s)^{-1} = \frac{-q_1 \psi(x, 1)}{C_1 e^{-\tau A_1}(sI - \bar{A}_1)^{-1} B_1} \quad (96)$$

to make (95) hold. It follows that (93) holds by rewriting (95) in the time domain. $h_3(\tilde{v}(2, t); x)$ can then be obtained by (46), (96). Inserting (83)–(84) into (77) along (87)–(88), applying (89) in Wang and Krstic (2019b), (91), we have

$$\begin{aligned} \tilde{z}_t(x, t) &+ q_1 \tilde{z}_x(x, t) + c_1 \tilde{w}(x, t) + c_1 \tilde{z}(x, t) + h_2(\tilde{v}(2, t); x) \\ &= q_1 \phi(x, 1) \tilde{\alpha}(1, t) + h_2(\tilde{v}(2, t); x) = 0 \end{aligned} \quad (97)$$

of which the detailed calculation is shown in (B.2) in Wang and Krstic (2019b). Therefore, $h_2(\tilde{v}(2, t); x)$ should satisfy

$$q_1 \phi(x, 1) \tilde{\alpha}(1, t) + h_2(\tilde{v}(2, t); x) = 0 \quad (98)$$

where $\tilde{\alpha}(1, t) = \tilde{z}(1, t)$ from (84) is used. Taking Laplace transform of (98) and recalling (45), (67), we have

$$\begin{aligned} q_1 \phi(x, 1) \tilde{z}(1, s) + H_2(s; x) \tilde{v}(2, s) \\ = (q_1 \phi(x, 1) + H_2(s; x) r(s)) \tilde{z}(1, s) = 0. \end{aligned} \quad (99)$$

$H_2(s; x)$ is obtained as

$$H_2(s; x) = -q_1 \phi(x, 1) r(s)^{-1} = \frac{-q_1 \phi(x, 1)}{C_1 e^{-\tau A_1}(sI - \bar{A}_1)^{-1} B_1} \quad (100)$$

to ensure (97) holds. $h_2(\tilde{v}(2, t); x)$ can thus be defined by (100), (45). Boundary conditions (76), (79) follow directly from inserting $x = 0, x = 1$ into (83)–(84) and applying (87) in Wang and Krstic (2019b), (86), (89). ODEs (75), (80) are obtained directly from (85), (90) via (83), (84) respectively. The second conversion is thus completed and two PDEs (77)–(78) are decoupled now, which can be seen in (87)–(88).

3.3. Third transformation

In order to decouple the ODE (85) with the PDEs and rebuild the ODE in a stable form, we intend to convert the second intermediate system (85)–(90) to the following target observer error system

$$\dot{\tilde{Z}}(t) = \bar{A}_0 \tilde{Z}(t), \quad (101)$$

$$\tilde{\alpha}(0, t) = C_0 \tilde{Z}(t), \quad (102)$$

$$\tilde{\alpha}_t(x, t) = -q_1 \tilde{\alpha}_x(x, t) - c_1 \tilde{\alpha}(x, t), \quad (103)$$

$$\dot{\tilde{Y}}(t) = \bar{A}_1 \tilde{Y}(t) + B_1 \tilde{\alpha}(1, t), \quad (104)$$

for $t \geq t_0 = \tau + \frac{1}{q_2}$, where \bar{A}_0 is a Hurwitz matrix defined in (8). Please note that $\tilde{\beta}(x, t) \equiv 0$ after $t_0 = \tau + \frac{1}{q_2}$ recalling (88)–(89), and then $\tilde{\beta}(x, t)$ can be removed for brevity. (85)–(90) can thus be rewritten as

$$\dot{\tilde{X}}(t) = A_0 \tilde{X}(t) - E_0 \int_0^1 \psi(0, y) \tilde{\alpha}(y, t) dy + h_1(\tilde{v}(2, t)), \quad (105)$$

$$\tilde{\alpha}(0, t) = C_0 \tilde{X}(t) - \int_0^1 C_0 K_1(y) \tilde{\alpha}(y, t) dy, \quad (106)$$

$$\tilde{\alpha}_t(x, t) = -q_1 \tilde{\alpha}_x(x, t) - c_1 \tilde{\alpha}(x, t), \quad (107)$$

$$\dot{\tilde{Y}}(t) = \bar{A}_1 \tilde{Y}(t) + B_1 \tilde{\alpha}(1, t), \quad (108)$$

for $t \geq t_0$. Note that (107)–(108) are the same as (103)–(104). We thus only need to convert (105)–(106) to (101)–(102). The following transformation

$$\tilde{Z}(t) = \tilde{X}(t) - \int_0^1 K_1(y) \tilde{\alpha}(y, t) dy \quad (109)$$

is applied to complete the conversion, where $K_1(y)$ satisfies (115)–(116) in Wang and Krstic (2019b). Note that the conditions of $\psi(x, y), \phi(x, y), K_1(y)$, i.e., (86)–(89), (115)–(116) in Wang and Krstic (2019b) is a 2×2 hyperbolic PDE-ODE system, which is a scalar case of the well-posed kernel equations (17)–(23) in Di Meglio, Bribiesca, Hu, and Krstic (2018) (setting dimensions in Di Meglio et al. (2018) as 1). Therefore, the kernels $\psi(x, y), \phi(x, y)$ in (83)–(84) and $K_1(y)$ in (109) are well-defined. In what follows, $H_1(s)$ is determined in matching (105)–(106) and (101)–(102) via (109). Submitting (109) into (101), applying (105)–(107), (115)–(116) in Wang and Krstic (2019b), we have

$$\begin{aligned} & \dot{\tilde{Z}}(t) - \bar{A}_0 \tilde{Z}(t) \\ &= h_1(\tilde{v}(2, t)) + q_1 K_1(1) \tilde{\alpha}(1, t) = 0, \quad t \geq t_0, \end{aligned} \quad (110)$$

of which the detailed calculation is shown in (117) in Wang and Krstic (2019b). Thus $H_1(s)$ which determines $h_1(\tilde{v}(2, t))$ can be solved from

$$h_1(\tilde{v}(2, t)) + q_1 K_1(1) \tilde{z}(1, t) = 0 \quad (111)$$

where $\tilde{\alpha}(1, t) = \tilde{z}(1, t)$ according to (84) is used. Writing (111) in the frequency domain and applying (44), (67) yield

$$\begin{aligned} & H_1(s) \tilde{v}(2, s) + q_1 K_1(1) \tilde{z}(1, s) \\ &= (H_1(s) r(s) + q_1 K_1(1)) \tilde{z}(1, s) = 0. \end{aligned} \quad (112)$$

$H_1(s)$ is solved as

$$H_1(s) = -q_1 K_1(1) r(s)^{-1} = \frac{-q_1 K_1(1)}{C_1 e^{-\tau \bar{A}_1} (sI - \bar{A}_1)^{-1} B_1}. \quad (113)$$

It follows that (110) holds by rewriting (112) in the time domain. $h_1(\tilde{v}(2, t))$ can then be defined via (44), (113). Inserting (109) into (106), it is straightforward to obtain (102). Therefore, (101)–(102) is converted from (105)–(106) through (109) for $t \geq t_0$. The third transformation is completed and the ODE (101) is independent and exponentially stable now.

After the above three transformations, we have converted the original observer error system (36)–(43) to the target observer error system (101)–(104) (for $t \in [t_0, \infty)$, $\tilde{\eta}(x, t) \equiv 0$ (81)–(82) and $\tilde{\beta}(x, t) \equiv 0$ (88)–(89) are removed for brevity). Because the original observer error system (36)–(43) is bounded in the finite time $t \in [0, t_0]$, we prove the exponential stability of (36)–(43) for $t \in [t_0, \infty)$ in the next subsection.

Note that dynamics H_i determined above are some dynamic extensions, of which the states are dynamic output injections in the observer (27)–(34), denoted as follows

$$y_1(t) = h_1(\tilde{v}(2, t)), \quad y_2(x, t) = h_2(\tilde{v}(2, t); x), \quad (114)$$

$$y_3(x, t) = h_3(\tilde{v}(2, t); x), \quad (115)$$

$$y_4(t) = h_4(\tilde{v}(2, t)), \quad y_5(x, t) = h_5(\tilde{v}(2, t); x), \quad (116)$$

which are proved as exponentially convergent to zero as well in the next subsection.

Remark 2. $H_i(s) \tilde{v}(2, s)$ usually generates time-derivatives of $\tilde{v}(2, t)$ in the time domain, which often appears in using the frequency-domain design approach. In practice, one way to avoid taking the time derivatives which may lead to measurement noise amplification is measuring n -order time-derivative states $\partial_t^n \tilde{v}(2, t)$ and calculating $\tilde{v}(2, t)$ by n times integrations of $\partial_t^n \tilde{v}(2, t)$, which is actually equal to multiplying $H_i(s)$ by $\frac{1}{s^n}$ to make $H_i(s)$ proper. As shown in an application case of control of DCV in Section 6, payload oscillation acceleration is measured and the velocity is calculated by integrating with the known initial conditions. Measuring acceleration is a prevalent method in many mechanical systems, because the acceleration sensor is cheaper and far easier to manufacture and install (Basturk & Krstic, 2014).

3.4. Stability analysis of the observer errors

Notation: Supposing $u(x, t)$ is on a spatial domain $x \in [d_1, d_2]$, $\|u(\cdot, t)\| = \sqrt{\int_{d_1}^{d_2} u(x, t)^2 dx}$ denotes the L^2 norm and $\|u(\cdot, t)\|_\infty = \sup_{x \in [d_1, d_2]} \{|u(x, t)|\}$ denotes the ∞ -norm. $|\cdot|$ denotes the Euclidean norm.

Theorem 1. For any initial data $(\tilde{z}(x, 0), \tilde{w}(x, 0), \tilde{v}(x, 0), \tilde{X}(0), \tilde{Y}(0)) \in L^2(0, 1) \times L^2(0, 1) \times L^2(1, 2) \times \mathbb{R}^n \times \mathbb{R}^m$, internal exponential stability of the observer error system (36)–(43) holds in the sense of the norm

$$\begin{aligned} & \|\tilde{z}(\cdot, t)\|_\infty + \|\tilde{w}(\cdot, t)\|_\infty + \|\tilde{v}(\cdot, t)\|_\infty + |\tilde{X}(t)| + |\tilde{Y}(t)| + |y_1(t)| \\ &+ |y_4(t)| + \|y_2(\cdot, t)\|_\infty + \|y_3(\cdot, t)\|_\infty + \|y_5(\cdot, t)\|_\infty \end{aligned} \quad (117)$$

with the decay rate being adjustable by L_0, L_1 .

Proof. The stability of the original observer error system can be obtained by analyzing the stability of the target observer error system (101)–(104) and using the invertibility of the transformations. (101)–(104) is a cascade of $\tilde{Z}(t)$ into $\tilde{\alpha}(\cdot, t)$ into $\tilde{Y}(t)$. From (101), $\tilde{Z}(t)$ is exponentially convergent to zero because \bar{A}_0 is Hurwitz. With the method of characteristics as Deutscher et al. (2018) it is easy to show that $\tilde{\alpha}(x, t)$ in the PDE subsystem (101)–(102) are exponentially convergent to zero. Because \bar{A}_1 is Hurwitz, we have $\tilde{Y}(t)$ is exponentially convergent to zero. The decay rate λ_e of (101)–(104) depends on the decay rate of the ODEs $\tilde{Z}(t), \tilde{Y}(t)$. In other words, the decay rate λ_e is adjustable by L_0, L_1 according to (8)–(9). Recalling $\tilde{\eta}(x, t) \equiv 0$ and $\tilde{\beta}(x, t) \equiv 0$ after $t_0 = \frac{1}{q_2} + \tau$, we obtain $\tilde{\Omega}(t) = \|\tilde{\alpha}(\cdot, t)\|_\infty + \|\tilde{\beta}(\cdot, t)\|_\infty + \|\tilde{\eta}(\cdot, t)\|_\infty + |\tilde{Z}(t)| + |\tilde{Y}(t)|$ is bounded by an exponential decay with the decay rate λ_e for $t \geq t_0$. Note that the transient in the finite time $[0, t_0]$ can be bounded by an arbitrarily fast decay rate considering a trade off between the decay rate and the overshoot coefficient, i.e., the higher the decay rate, the higher the overshoot coefficient. Therefore, we conclude the exponential stability in the sense of $\tilde{\Omega}(t)$ being bounded by an exponential decay rate λ_e with some overshoot coefficients for $t \geq 0$. Applying the transformation (49), (109) and (83)–(84), we respectively have $\|\tilde{v}(\cdot, t)\|_\infty \leq \gamma_{1a} (\|\tilde{\eta}(\cdot, t)\|_\infty + |\tilde{Y}(t)|), |\tilde{X}(t)| \leq \gamma_{1b} (\|\tilde{\alpha}(\cdot, t)\|_\infty + |\tilde{Z}(t)|), \|\tilde{z}(\cdot, t)\|_\infty + \|\tilde{w}(\cdot, t)\|_\infty \leq \gamma_{1c} (\|\tilde{\alpha}(\cdot, t)\|_\infty + \|\tilde{\beta}(\cdot, t)\|_\infty)$, for some positive $\gamma_{1a}, \gamma_{1b}, \gamma_{1c}$.

According to (44)–(48), (113), (100), (96), (74), (71), we know the output injection states $y_1(t), y_2(x, t), y_3(x, t), y_4(t), y_5(x, t)$ are the output states of the following extended dynamics:

$$H_1(s) = \frac{-q_1 K_1(1)}{C_1 e^{-\tau A_1}(sI - \bar{A}_1)^{-1} B_1}, \quad (118)$$

$$H_2(s; x) = \frac{-q_1 \phi(x, 1)}{C_1 e^{-\tau A_1}(sI - \bar{A}_1)^{-1} B_1}, \quad (119)$$

$$H_3(s; x) = \frac{-q_1 \psi(x, 1)}{C_1 e^{-\tau A_1}(sI - \bar{A}_1)^{-1} B_1}, \quad (120)$$

$$H_4(s) = \frac{q + C_1(sI - \bar{A}_1)^{-1} B_1}{C_1 e^{-\tau A_1}(sI - \bar{A}_1)^{-1} B_1}, \quad (121)$$

$$H_5(s; x) = C_1 e^{-\tau A_1(x-1)} \Gamma_1 - \frac{C_1 e^{-\tau A_1(x-1)} B_1}{C_1 e^{-\tau A_1}(sI - \bar{A}_1)^{-1} B_1}, \quad (122)$$

of which the input signal is $\tilde{v}(2, t)$ which is exponentially convergent to zero. Recalling Lemma 1, we know there is not pole in the closed right-half plane in the transfer function (118)–(122), the exponential convergence of $\|y_1(t)\|, \|y_2(x, t)\|_\infty, \|y_3(x, t)\|_\infty, \|y_4(t)\|, \|y_5(x, t)\|_\infty$ are thus obtained. Note that $x \in [0, 1]$ is just a parameter in the transfer functions (119), (120), (122) and the stability result would not be affected. ■

4. Output-feedback control design

In the last section, we have built the observer which can compensate the time-delay in the output measurement $y_{\text{out}}(t)$ of the distal ODE, which is the only one measurement used in the observer, to track the states of the overall sandwiched PDE system (1)–(7). In this section, we design an output-feedback control law $U(t)$ based on the observer (27)–(34) by using backstepping transformations and frequency-domain designs.

First, two transformations are introduced to transform the observer (27)–(34) to a target system (139)–(146), which is in a stable-like form except for the proximal ODE which is influenced by perturbations originating from the PDEs and distal ODE. Representing this “target system” in the frequency domain by using Laplace transform, the algebraic relationships (160)–(166) between the states of the proximal ODE and the states of the PDEs and distal ODE are obtained. Inserting these algebraic relationships to rewrite the perturbations in the proximal ODE, a new ODE (171) without external perturbations can be built in the frequency domain, where the control input to exponentially stabilize this ODE can be designed.

4.1. First transformation

The aim of the first transformation is to remove the source terms in the PDE domain $x \in [0, 1]$, i.e., couplings in (29)–(30), and to build the state matrix of the distal ODE (32) as a Hurwitz matrix. A PDE backstepping transformation in the following form (Di Meglio et al., 2018)

$$\begin{aligned} \alpha(x, t) &= \hat{z}(x, t) - \int_x^1 K_3(x, y) \hat{z}(y, t) dy \\ &\quad - \int_x^1 J_3(x, y) \hat{w}(y, t) dy - \gamma(x) \hat{Y}(t), \end{aligned} \quad (123)$$

$$\begin{aligned} \beta(x, t) &= \hat{w}(x, t) - \int_x^1 K_2(x, y) \hat{z}(y, t) dy \\ &\quad - \int_x^1 J_2(x, y) \hat{w}(y, t) dy - \lambda(x) \hat{Y}(t) \end{aligned} \quad (124)$$

is introduced, where the kernels $K_3(x, y), J_3(x, y), \gamma(x), K_2(x, y), J_2(x, y), \lambda(x)$ are to be determined later, to convert (27)–(34) to the following intermediate system:

$$\begin{aligned} \dot{\hat{X}}(t) &= A_0 \hat{X}(t) + E_0 \beta(0, t) + \int_0^1 \bar{K}_4(x) \alpha(x, t) dx \\ &\quad + \int_0^1 \bar{K}_5(x) \beta(x, t) dx + \bar{K}_6 \hat{Y}(t) \\ &\quad + B_0 U(t) + h_1(\tilde{v}(2, t)), \end{aligned} \quad (125)$$

$$\begin{aligned} \alpha(0, t) &= p \beta(0, t) + C_0 \hat{X}(t) + \int_0^1 \bar{K}_1(x) \alpha(x, t) dx \\ &\quad + \bar{K}_3 \hat{Y}(t) + \int_0^1 \bar{K}_2(x) \beta(x, t) dx, \end{aligned} \quad (126)$$

$$\begin{aligned} \alpha_t(x, t) &= -q_1 \alpha_x(x, t) - c_1 \alpha(x, t) - \gamma(x) \Gamma_1 \tilde{v}(2, t) \\ &\quad - \int_x^1 J_2(x, y) h_3(\tilde{v}(2, t); y) dy \\ &\quad - \int_x^1 K_3(x, y) h_2(\tilde{v}(2, t); y) dy \\ &\quad + h_2(\tilde{v}(2, t); x) - q_2 J_3(x, 1) h_4(\tilde{v}(2, t)), \end{aligned} \quad (127)$$

$$\begin{aligned} \beta_t(x, t) &= q_2 \beta_x(x, t) - c_2 \beta(x, t) \\ &\quad - \lambda(x) \Gamma_1 \tilde{v}(2, t) - \int_x^1 J_2(x, y) h_3(\tilde{v}(2, t); y) dy \\ &\quad - \int_x^1 K_2(x, y) h_2(\tilde{v}(2, t); y) dy \\ &\quad + h_3(\tilde{v}(2, t); x) - q_2 J_2(x, 1) h_4(\tilde{v}(2, t)), \end{aligned} \quad (128)$$

$$\beta(1, t) = q \alpha(1, t) + h_4(\tilde{v}(2, t)), \quad (129)$$

$$\dot{\hat{Y}}(t) = \hat{A}_1 \hat{Y}(t) + B_1 \alpha(1, t) + \Gamma_1 \tilde{v}(2, t), \quad (130)$$

$$\hat{v}(1, t) = C_1 \hat{Y}(t), \quad (131)$$

$$\hat{v}_t(x, t) = -\frac{1}{\tau} \hat{v}_x(x, t) + h_5(\tilde{v}(2, t); x), \quad (132)$$

where \hat{A}_1 is a Hurwitz matrix by choosing the control parameter F_1 according to Assumption 2. $\bar{K}_1(x), \bar{K}_2(x), \bar{K}_3, \bar{K}_4(x), \bar{K}_5(x), \bar{K}_6$ should satisfy (140)–(145) in Wang and Krstic (2019b), which are obtained by matching (125)–(126) and (27)–(28) via (123)–(124) (please see Step 4 in the Appendix-A of Wang and Krstic (2019b) for the details). By matching (127)–(130) and (29)–(32) (the detailed process is shown in Steps. 1–3 in the Appendix-A of Wang and Krstic (2019b)), the conditions on the kernels $K_3(x, y), J_3(x, y), \gamma(x), K_2(x, y), J_2(x, y), \lambda(x)$ in the transformations (123)–(124) are obtained as (146)–(157) in Wang and Krstic (2019b), of which the well-posedness is given in Lemma 2 in Wang and Krstic (2019b).

Similarly, the inverse transformation can be obtained as

$$\begin{aligned} \hat{z}(x, t) &= \alpha(x, t) - \int_x^1 \mathcal{M}(x, y) \alpha(y, t) dy \\ &\quad - \int_x^1 \mathcal{N}(x, y) \beta(y, t) dy - \mathcal{G}(x) \hat{Y}(t), \end{aligned} \quad (133)$$

$$\begin{aligned} \hat{w}(x, t) &= \beta(x, t) - \int_x^1 \mathcal{D}(x, y) \alpha(y, t) dy \\ &\quad - \int_x^1 \mathcal{T}(x, y) \beta(y, t) dy - \mathcal{P}(x) \hat{Y}(t), \end{aligned} \quad (134)$$

where $\mathcal{M}(x, y), \mathcal{N}(x, y), \mathcal{G}(x), \mathcal{D}(x, y), \mathcal{T}(x, y), \mathcal{P}(x)$ are kernels which can be determined through a similar process in the Appendix-A of Wang and Krstic (2019b). The first transformation in the control design is completed.

4.2. Second transformation

In order to remove the last three terms in the boundary condition (126) and form a Hurwitz matrix of the proximal ODE (125), we introduce the second transformation

$$\begin{aligned} \hat{Z}(t) &= \hat{X}(t) + C_0^+ \int_0^1 \bar{K}_1(x) \alpha(x, t) dx \\ &+ C_0^+ \int_0^1 \bar{K}_2(x) \beta(x, t) dx + C_0^+ \bar{K}_3 \hat{Y}(t), \end{aligned} \quad (135)$$

where C_0^+ denotes the Moore–Penrose right inverse of C_0 . Note that because C_0 is full-row rank (with rank equal to 1), a right inverse exists for C_0 , i.e., $C_0 C_0^+ = I$. A choice of C_0^+ is $C_0^+ = C_0^T (C_0 C_0^T)^{-1}$. Using (135), then (125)–(126) is converted to

$$\begin{aligned} \dot{\hat{Z}}(t) &= \hat{A}_0 \hat{Z}(t) + q_1 C_0^+ \bar{K}_1(0) C_0 \hat{Z}(t) + B_0 \bar{U}(t) \\ &+ M_Y \hat{Y}(t) + \int_0^1 M_\alpha(x) \alpha(x, t) dx + \int_0^1 M_\beta(x) \beta(x, t) dx \\ &+ N_1 \alpha(1, t) + N_2 \beta(0, t) + \mathcal{H}[h_1(\tilde{v}(2, t)), h_2(\tilde{v}(2, t); x), \end{aligned} \quad (136)$$

$$h_3(\tilde{v}(2, t); x), h_4(\tilde{v}(2, t)), h_5(\tilde{v}(2, t); x), \tilde{v}(2, t)],$$

$$\alpha(0, t) = p \beta(0, t) + C_0 \hat{Z}(t), \quad (137)$$

where

$$\bar{U}(t) = U(t) - F_0 \hat{Z}(t), \quad (138)$$

and \hat{A}_0 is Hurwitz by choosing the control parameter F_0 considering Assumption 2. In (136), the expression of $\mathcal{H}[h_1(\tilde{v}(2, t)), h_2(\tilde{v}(2, t); x), h_3(\tilde{v}(2, t); x), h_4(\tilde{v}(2, t)), h_5(\tilde{v}(2, t); x), \tilde{v}(2, t)]$ is shown in (163) of Wang and Krstic (2019b), and $N_1, N_2, M_\alpha(x), M_\beta(x), M_Y$ are shown in (165)–(169) of Wang and Krstic (2019b). We thus arrive at the target system consisting of (127)–(132), (136)–(137) includes the dynamic output injections in \mathcal{H} . Considering Theorem 1 and (114)–(116), we know dynamic output injections $h_1(\tilde{v}(2, t)), h_2(\tilde{v}(2, t); x), h_3(\tilde{v}(2, t); x), h_4(\tilde{v}(2, t)), h_5(\tilde{v}(2, t); x)$ and $\Gamma_1 \tilde{v}(2, t)$ can be regarded as zero, i.e., $\mathcal{H} = 0$, for brevity. Therefore, the target system (127)–(132), (136)–(137) can be rewritten as

$$\begin{aligned} \dot{\hat{Z}}(t) &= \hat{A}_0 \hat{Z}(t) + q_1 C_0^+ \bar{K}_1(0) C_0 \hat{Z}(t) \\ &+ M_Y \hat{Y}(t) + \int_0^1 M_\alpha(x) \alpha(x, t) dx + \int_0^1 M_\beta(x) \beta(x, t) dx \\ &+ N_1 \alpha(1, t) + N_2 \beta(0, t) + B_0 \bar{U}(t), \end{aligned} \quad (139)$$

$$\alpha(0, t) = p \beta(0, t) + C_0 \hat{Z}(t), \quad (140)$$

$$\alpha_t(x, t) = -q_1 \alpha_x(x, t) - c_1 \alpha(x, t), \quad x \in [0, 1] \quad (141)$$

$$\beta_t(x, t) = q_2 \beta_x(x, t) - c_2 \beta(x, t), \quad x \in [0, 1] \quad (142)$$

$$\beta(1, t) = q \alpha(1, t), \quad (143)$$

$$\dot{\hat{Y}}(t) = \hat{A}_1 \hat{Y}(t) + B_1 \alpha(1, t), \quad (144)$$

$$\hat{v}(1, t) = C_1 \hat{Y}(t), \quad (145)$$

$$\hat{v}_t(x, t) = -\frac{1}{\tau} \hat{v}_x(x, t), \quad x \in [1, 2]. \quad (146)$$

4.3. Control design in frequency domain

In the last two subsections, the system (27)–(34) is converted to the target system (139)–(146), through the two transformations (123)–(124) and (135). In this section, the control $\bar{U}(t)$ in (139) of the target system (139)–(146) will be designed in the frequency domain by using Laplace transform.

Taking Laplace transform of (139)–(146), we have

$$(sI - \hat{A}_0) \hat{Z}(s) = q_1 C_0^+ \bar{K}_1(0) C_0 \hat{Z}(s) + M_Y \hat{Y}(s)$$

$$\begin{aligned} &+ \int_0^1 M_\alpha(x) \alpha(x, s) dx + \int_0^1 M_\beta(x) \beta(x, s) dx \\ &+ N_1 \alpha(1, s) + N_2 \beta(0, s) + B_0 \bar{U}(s), \end{aligned} \quad (147)$$

$$\alpha(0, s) = p \beta(0, s) + C_0 \hat{Z}(s), \quad (148)$$

$$s \alpha(x, s) = -q_1 \alpha_x(x, s) - c_1 \alpha(x, s), \quad (149)$$

$$s \beta(x, s) = q_2 \beta_x(x, s) - c_2 \beta(x, s), \quad (150)$$

$$\beta(1, s) = q \alpha(1, s), \quad (151)$$

$$(sI - \hat{A}_1) \hat{Y}(s) = B_1 \alpha(1, s), \quad (152)$$

$$\hat{v}(1, s) = C_1 \hat{Y}(s), \quad (153)$$

$$s \hat{v}(x, s) = -\frac{1}{\tau} \hat{v}_x(x, s). \quad (154)$$

Note: for brevity, we consider all zero initial conditions while taking Laplace transform (arbitrary initial conditions could be incorporated into the stability statement through an expanded analysis which is routine).

Defining

$$h(s) = 1 - p q e^{-(\frac{c_2}{q_2} + \frac{c_1}{q_1})s} e^{-(\frac{1}{q_2} + \frac{1}{q_1})s}, \quad (155)$$

according to (148)–(154) and Section 3.2 in Di Meglio et al. (2020), we obtain the following algebraic relationships between $C_0 \hat{Z}(s)$ and other states in (148)–(154):

$$h(s) \alpha(x, s) = e^{-\frac{c_1-s}{q_1} x} C_0 \hat{Z}(s), \quad (156)$$

$$h(s) \beta(x, s) = q e^{-\frac{(c_2+s)}{q_2} (1-x) - \frac{(c_1+s)}{q_1}} C_0 \hat{Z}(s), \quad (157)$$

$$h(s) \hat{v}(x, s) = C_1 (sI - \hat{A}_1)^{-1} B_1 e^{-\frac{c_1-s}{q_1} - \tau(x-1)s} C_0 \hat{Z}(s), \quad (158)$$

$$h(s) \hat{v}(1, s) = C_1 (sI - \hat{A}_1)^{-1} B_1 e^{-\frac{(c_1+s)}{q_1}} C_0 \hat{Z}(s), \quad (159)$$

$$h(s) \alpha(0, s) = C_0 \hat{Z}(s), \quad (160)$$

$$h(s) \beta(1, s) = q e^{-\frac{(c_1+s)}{q_1}} C_0 \hat{Z}(s), \quad (161)$$

$$h(s) \beta(0, s) = q e^{-\frac{(c_2+s)}{q_2} - \frac{(c_1+s)}{q_1}} C_0 \hat{Z}(s), \quad (162)$$

$$h(s) \alpha(1, s) = e^{-\frac{(c_1+s)}{q_1}} C_0 \hat{Z}(s), \quad (163)$$

$$h(s) \hat{Y}(s) = (sI - \hat{A}_1)^{-1} B_1 e^{-\frac{(c_1+s)}{q_1}} C_0 \hat{Z}(s), \quad (164)$$

$$\begin{aligned} h(s) \int_0^1 M_\beta(y) \beta(y, s) dy \\ = \int_0^1 M_\beta(y) q e^{-\frac{(c_2+s)}{q_2} (1-y) - \frac{(c_1+s)}{q_1}} dy C_0 \hat{Z}(s), \end{aligned} \quad (165)$$

$$\begin{aligned} h(s) \int_0^1 M_\alpha(y) \alpha(y, s) dy \\ = \int_0^1 M_\alpha(y) e^{-\frac{(c_1+s)}{q_1} y} dy C_0 \hat{Z}(s). \end{aligned} \quad (166)$$

Multiplying both sides of (147) by scalar $h(s)$, and substituting (160)–(166) therein yields

$$\begin{aligned} h(s) (sI - \hat{A}_0) \hat{Z}(s) &= h(s) B_0 \bar{U}(s) + h(s) q_1 C_0^+ \bar{K}_1(0) C_0 \hat{Z}(s) \\ &+ M_Y (sI - \hat{A}_1)^{-1} B_1 e^{-\frac{(c_1+s)}{q_1}} C_0 \hat{Z}(s) \\ &+ \int_0^1 M_\alpha(y) e^{-\frac{(c_1+s)}{q_1} y} dy C_0 \hat{Z}(s) \\ &+ \int_0^1 M_\beta(y) q e^{-\frac{(c_2+s)}{q_2} (1-y) - \frac{(c_1+s)}{q_1}} dy C_0 \hat{Z}(s) \\ &+ N_1 e^{-\frac{(c_1+s)}{q_1}} C_0 \hat{Z}(s) + N_2 q e^{-\frac{(c_2+s)}{q_2} - \frac{(c_1+s)}{q_1}} C_0 \hat{Z}(s). \end{aligned} \quad (167)$$

Recalling Assumption 1, we know $h(s)$ is nonzero for any $s \in \mathbb{C}$, $\Re(s) \geq 0$ and then $h(s)$ has an inverse $h(s)^{-1}$. Multiplying both

sides of (167) by $h(s)^{-1}$ and defining

$$\hat{\xi}(t) = C_0 \hat{Z}(t), \quad (168)$$

(167) is then rewritten as

$$\begin{aligned} (sI - \hat{A}_0) \hat{Z}(s) &= B_0 \bar{U}(s) + q_1 C_0^+ \bar{K}_1(0) \hat{\xi}(s) \\ &+ h(s)^{-1} M_Y (sI - \hat{A}_1)^{-1} B_1 e^{-\frac{(c_1+s)}{q_1}} \hat{\xi}(s) \\ &+ h(s)^{-1} \int_0^1 M_\alpha(y) e^{-\frac{(c_1+s)}{q_1} y} dy \hat{\xi}(s) \\ &+ h(s)^{-1} \int_0^1 M_\beta(y) q e^{-\frac{(c_2+s)}{q_2} (1-y) - \frac{(c_1+s)}{q_1}} dy \hat{\xi}(s) \\ &+ h(s)^{-1} N_1 e^{-\frac{(c_1+s)}{q_1}} \hat{\xi}(s) + h(s)^{-1} N_2 q e^{-\frac{(c_2+s)}{q_2} - \frac{(c_1+s)}{q_1}} \hat{\xi}(s) \end{aligned}$$

for any $s \in \mathbb{C}$, $\Re(s) \geq 0$. Defining

$$\begin{aligned} G(s) &= q_1 C_0^+ \bar{K}_1(0) + h(s)^{-1} \left[M_Y (sI - \hat{A}_1)^{-1} B_1 e^{-\frac{(c_1+s)}{q_1}} \right. \\ &+ \int_0^1 M_\alpha(y) e^{-\frac{(c_1+s)}{q_1} y} dy + \int_0^1 M_\beta(y) q e^{-\frac{(c_2+s)}{q_2} (1-y) - \frac{(c_1+s)}{q_1}} dy \\ &\left. + N_1 e^{-\frac{(c_1+s)}{q_1}} + N_2 q e^{-\frac{(c_2+s)}{q_2} - \frac{(c_1+s)}{q_1}} \right] \end{aligned} \quad (169)$$

which is a stable, proper transfer matrix, we have

$$(sI - \hat{A}_0) \hat{Z}(s) = G(s) \hat{\xi}(s) + B_0 \bar{U}(s). \quad (170)$$

Recalling \hat{A}_0 being Hurwitz, $\det(sI - \hat{A}_0)$ does not have any zeros in the closed right-half plane. Then the matrix $(sI - \hat{A}_0)$ is invertible for any $s \in \mathbb{C}$, $\Re(s) \geq 0$. Multiplying both sides of (170) $C_0(sI - \hat{A}_0)^{-1}$, we obtain

$$C_0 \hat{Z}(s) = C_0(sI - \hat{A}_0)^{-1} G(s) \hat{\xi}(s) + C_0(sI - \hat{A}_0)^{-1} B_0 \bar{U}(s).$$

That is

$$\hat{\xi}(s) = C_0(sI - \hat{A}_0)^{-1} G(s) \hat{\xi}(s) + W_0 \bar{U}(s), \quad (171)$$

where $W_0(s) = C_0(sI - \hat{A}_0)^{-1} B_0$. Recalling [Assumption 3](#) which is equivalent to the existence of a right inverse for W_0 . A possible choice is given by the Moore-Penrose right inverse $W_0^+(s) = W_0^T(s)(W_0(s)W_0^T(s))^{-1}$ ([Bou Saba et al., 2019](#)).

Choose $\bar{U}(s)$ in (171) as

$$\bar{U}(s) = -W_0^+(s)\Omega(s)C_0(sI - \hat{A}_0)^{-1} G(s) \hat{\xi}(s) = F(s) \hat{\xi}(s) \quad (172)$$

where a SISO low-pass filter $\Omega(s)$ satisfying

$$|1 - \Omega(j\omega)| < \frac{1}{\sup_{\omega \in R} \tilde{\sigma}(G(j\omega)) \tilde{\sigma}(C_0(j\omega I - \hat{A}_0)^{-1})}, \forall \omega \in R \quad (173)$$

is adopted to make sure $F(s)$ strictly proper. Note that because $G(s)$ is uniformly bounded in the closed right-half plane, $\sup_{\omega \in R} \tilde{\sigma}(G(j\omega))$ is bounded where $\tilde{\sigma}$ stands for the largest singular value. A low-pass filter $\Omega(s)$ always can be chosen to ensure $F(s)$ strictly proper and satisfy (173) concurrently, because there exists a ω_1 to make the right hand side of (173) larger than 1 at $\omega \geq \omega_1$ ($\sup_{\omega \in R} \tilde{\sigma}(G(j\omega))$ is bounded and $\tilde{\sigma}(C_0(j\omega I - \hat{A}_0)^{-1})$ can be small enough at sufficiently high frequencies), and thus (173) still holds even if the gain $|\Omega(j\omega)|$ of the low-pass filter is close to zero for $\omega \geq \omega_1$. It means that a choice of the cut-off frequency of the low-pass filter $\Omega(s)$ is ω_1 . Note that \bar{U} has been chosen as strictly proper by introducing the low-pass filter $\Omega(s)$, which means that the controller is robust to small input delays ([Bou Saba et al., 2019](#)).

Substituting (172) into (171), we have

$$\hat{\xi}(s) = (1 - \Omega(s))C_0(sI - \hat{A}_0)^{-1} G(s) \hat{\xi}(s) = \Phi(s) \hat{\xi}(s).$$

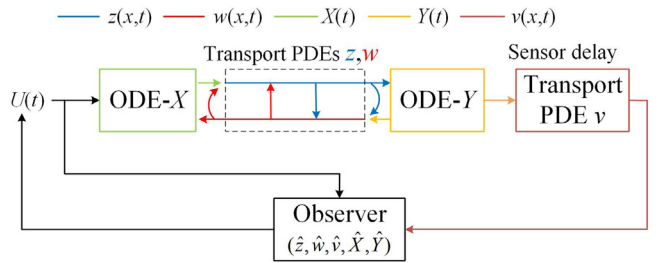


Fig. 2. Diagram of the closed-loop system.

That is

$$(1 - \Phi(s)) \hat{\xi}(s) = 0, \quad (174)$$

where

$$\begin{aligned} \tilde{\sigma}(\Phi(j\omega)) &\leq |1 - \Omega(j\omega)| \tilde{\sigma}(C_0(j\omega I - \hat{A}_0)^{-1}) \sup_{\omega \in R} \tilde{\sigma}(G(j\omega)) \\ &< 1 \end{aligned} \quad (175)$$

by recalling (173), which is a sufficient condition for exponential convergence to zero of $\hat{\xi}$. Considering (172), (138), $U(s)$ can be written as

$$\begin{aligned} U(s) &= \bar{U}(s) + F_0 \hat{Z}(s) \\ &= [F_0 - W_0^+(s)\Omega(s)C_0(sI - \hat{A}_0)^{-1} G(s)C_0] \hat{Z}(s), \end{aligned} \quad (176)$$

where inverse Laplace transform is required to represent $U(s)$ in the time domain considering implementation of the controller and \hat{Z} can be replaced as the observer states by (135), (123)–(124).

5. Stability analysis of the closed-loop system

The closed-loop system includes the plant (1)–(7), the observer (27)–(34) and the controller (176). The block diagram of the closed-loop system is shown in [Fig. 2](#). We have given [Theorem 1](#) showing the observer error states between the plant and the observer are exponentially convergent to zero in the sense of the norm (117) in Section 3.4. Considering (35), in order to prove the exponential stability result of the closed-loop system, we present the next lemma to show the exponential stability of the system- $(\hat{z}(x, t), \hat{w}(x, t), \hat{v}(x, t), \hat{X}(t), \hat{Y}(t))$ (27)–(34) under the controller (176).

Lemma 2. For any initial data $(\hat{z}(x, 0), \hat{w}(x, 0), \hat{v}(x, 0), \hat{X}(0), \hat{Y}(0)) \in L^2(0, 1) \times L^2(0, 1) \times L^2(0, 1) \times L^2(1, 2) \times \mathbb{R}^n \times \mathbb{R}^m$, exponential stability of the system (27)–(34) under the controller (176) holds in the sense of the norm $\|\hat{z}(\cdot, t)\|_\infty + \|\hat{w}(\cdot, t)\|_\infty + \|\hat{v}(\cdot, t)\|_\infty + |\hat{X}(t)| + |\hat{Y}(t)|$ with the convergence rate being adjustable by F_0, F_1 .

Proof. We prove the exponential convergence of the states in the overall system based on the exponential convergence of $\hat{\xi}(t)$ by applying their algebraic relationships obtained in Section 4.3. According to exponential convergence to zero of $\hat{\xi}(t) = C_0 \hat{Z}(t)$, which is obtained from (174)–(175), recalling (156)–(158) and (164)–(166), we have $\alpha(x, t)$, $\beta(x, t)$, $\hat{v}(x, t)$, $\|\alpha(\cdot, t)\|$, $\|\beta(\cdot, t)\|$, $|\hat{Y}(t)|$ are exponentially convergent to zero, where the convergence rate is adjustable by F_0, F_1 considering (10)–(11). Substituting (172) into (170),

$$\begin{aligned} \hat{Z}(s) &= (sI - \hat{A}_0)^{-1} [G(s) - B_0 W_0^+ \Omega(s) C_0 (sI - \hat{A}_0)^{-1} G(s)] \hat{\xi}(s). \end{aligned} \quad (177)$$

Because $(sI - \hat{A}_0)^{-1}[G(s) - B_0 W_0^+ \mathcal{Q}(s) C_0 (sI - \hat{A}_0)^{-1} G(s)]$ is a (stable) proper transfer matrix, using the exponential convergence result of $\hat{\xi}$, we also obtain exponential convergence to zero of \hat{Z} via (177). Applying Cauchy–Schwarz inequality into the inverse transformations (133)–(134), and transformations (135), we obtain $|\hat{z}(x, t)| + |\hat{w}(x, t)| \leq \gamma_{2a}(|\alpha(x, t)| + |\beta(x, t)| + \|\alpha(\cdot, t)\| + \|\beta(\cdot, t)\| + |\hat{Y}(t)|)$ and $|\hat{X}(t)| \leq \gamma_{2b}(\|\alpha(\cdot, t)\| + \|\beta(\cdot, t)\| + |\hat{Y}(t)| + |\hat{Z}(t)|)$ for some positive γ_{2a}, γ_{2b} . Recalling the obtained exponential convergence of $\alpha(x, t), \beta(x, t), \|\alpha(\cdot, t)\|, \|\beta(\cdot, t)\|, |\hat{Y}(t)|, |\hat{Z}(t)|$, we thus obtain the exponential convergence to zero of $\hat{z}(x, t) + \hat{w}(x, t) + \hat{X}(t)$. Recalling the exponential convergence to zero of $|\hat{Y}(t)|$ and $\hat{v}(x, t)$, we obtain Lemma 2. ■

Theorem 2. For any initial data $(z(x, 0), w(x, 0), v(x, 0), X(0), Y(0)) \in L^2(0, 1) \times L^2(0, 1) \times L^2(1, 2) \times \mathbb{R}^n \times \mathbb{R}^m$, considering the closed-loop system including the plant (1)–(7), the observer (27)–(34) and the controller (176),

(1) The internal exponential stability holds in the sense of the norm

$$\|z(\cdot, t)\|_\infty + \|w(\cdot, t)\|_\infty + \|v(\cdot, t)\|_\infty + |X(t)| + |Y(t)| \\ \|z(\cdot, t)\|_\infty + \|\hat{w}(\cdot, t)\|_\infty + \|\hat{v}(\cdot, t)\|_\infty + |\hat{X}(t)| + |\hat{Y}(t)| \\ + |y_1(t)| + |y_4(t)| + \|y_2(\cdot, t)\|_\infty + \|y_3(\cdot, t)\|_\infty + \|y_5(\cdot, t)\|_\infty$$

with the convergence rate being adjustable by L_0, L_1, F_0, F_1 .

(2) There exist positive constants Γ_c and λ_c making the dynamic feedback control $U(t)$ bounded and exponentially convergent to zero in the sense of $|U(t)| \leq \Gamma_c e^{-\lambda_c t}$.

Proof. (1) Applying (35) and Cauchy–Schwarz inequality, recalling Theorem 1 and Lemma 2, we straightforwardly obtain (1) in Theorem 2.

(2) According to the control design in Section 4.3, we know $F(s) = W_0^+ \mathcal{Q}(s) C_0 (sI - \hat{A}_0)^{-1} G(s) C_0$ in (172) is strictly proper. It follows that $F_0 - W_0^+ \mathcal{Q}(s) C_0 (sI - \hat{A}_0)^{-1} G(s) C_0$ in (176) is a (stable) proper transfer function because F_0 is a constant matrix. Recalling (176) and the exponential convergence of \hat{Z} proved in Lemma 2, we obtain the exponential convergence to zero of the dynamic feedback control $U(t)$, which is a dynamic extension generated by utilizing the frequency-domain design approach. The proof of Theorem 2 is completed. ■

6. Application in control of a deepwater construction vessel

A DCV is used to place equipment to be installed at the predetermined location on the seafloor for off-shore oil drilling, which is shown in Fig. 3 and described in the first paragraph in Section 1. The equipment, referred to as payload, have to be installed accurately at the predetermined location with a tight tolerance, such as the permissible maximum tolerance for a typical subsea installation in How et al. (2011) is 2.5 m. In this section, we design an output-feedback control force at the crane to reduce oscillations of the long cable and position the payload in the target area, with compensating the time-delay in the measurement which is the oscillation acceleration of the payload, obtained by an acceleration sensor. The details of the application of the above theoretical results are presented in Wang and Krstic (2019b) due to the space limit. Note that we only consider one-dimensional oscillations of DCV and the end phase of the descending process, i.e., the cable length being constant. Control problems of two-dimensional coupled oscillations of DCV in the whole descending/ascending process with a time-varying-length cable are considered in Wang and Krstic (2020) which, however, is not a sandwiched system by neglecting the crane dynamics, and does not include delay compensation.

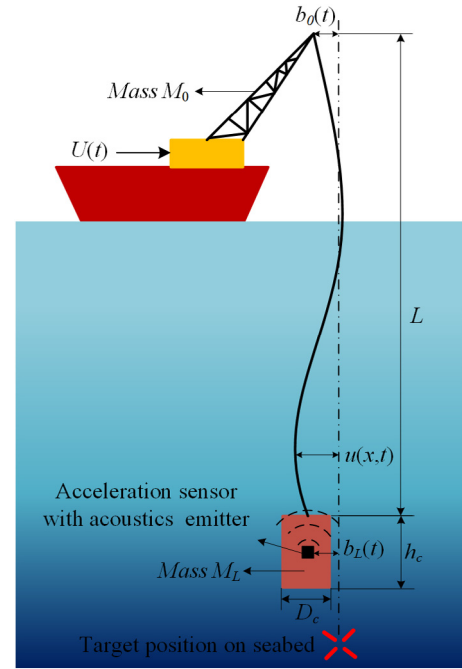


Fig. 3. Schematic of a DCV used in seafloor installation..

6.1. Modeling

DCV dynamics is modeled as (212)–(216) in Wang and Krstic (2019b), i.e., a wave PDE ($u(x, t)$ describing distributed transverse displacements along the cable) sandwiched by two ODEs ($b_0(t), b_L(t)$ represent transverse displacements of the onboard crane and the payload). The details of obtaining the DCV model- $(u(x, t), b_0(t), b_L(t))$ are shown in Sec. 6.1.1 in Wang and Krstic (2019b) and the physical parameters from How et al. (2011) are given in Table 2. Apply Riemann transformations:

$$z(x, t) = u_t(x, t) - \sqrt{\frac{T_0}{\rho}} u_x(x, t), \quad (178)$$

$$w(x, t) = u_t(x, t) + \sqrt{\frac{T_0}{\rho}} u_x(x, t) \quad (179)$$

where T_0 is static tension defined as $T_0 = M_L g - F_{buoyant}$ with $F_{buoyant} = \frac{1}{4}\pi D_c^2 h_c \rho_s g$, and defining new variables $X(t) = \dot{b}_0(t)$, $Y(t) = \dot{b}_L(t)$, (212)–(216) in Wang and Krstic (2019b) can be rewritten as

$$\dot{X}(t) = A_0 X(t) + E_0 w(0, t) + B_0 U(t), \quad (180)$$

$$z(0, t) = p w(0, t) + C_0 X(t), \quad (181)$$

$$z_t(x, t) = -q_1 z_x(x, t) - c_1(z(x, t) + w(x, t)) + f(x, t), \quad (182)$$

$$w_t(x, t) = q_2 w_x(x, t) - c_2(z(x, t) + w(x, t)) + f(x, t), \quad (183)$$

$$w(L, t) = qz(L, t) + C_1 Y(t), \quad (184)$$

$$\dot{Y}(t) = A_1 Y(t) + B_1 z(1, t) + f_L(t), \quad (185)$$

$$y_{\text{out}}(t) = C_1 Y(t - \tau), \quad (186)$$

where $y_{\text{out}}(t)$ is the delayed measurement output and $y_{\text{out}}(t) = 0, t \in [0, \tau]$ because the sensing signal has not been received. The observer and controller design in the next subsection is based on (180)–(186) except for the ocean current disturbances $f(z, t), f_L(t)$, i.e., external drag forces at the cable and payload, which are regarded as model uncertainties in the simulation

Table 2

Physical parameters of the DCV.

Parameters (units)	Values
Cable length L (m)	1000
Cable diameter R_D (m)	0.2
Cable effective Young's Modulus E (N/m ²)	4.0×10^9
Cable linear density ρ (kg/m)	8.02
Crane mass M_0 (kg)	1.0×10^6
Payload mass M_L (kg)	4.0×10^5
Gravitational acceleration g (m/s ²)	9.8
Cable material damping coefficient d_c (N s/m)	0.5
Height of payload modeled as a cylinder h_c (m)	10
Diameter of payload modeled as a cylinder D_c (m)	5
Damping coefficient at payload d_L (N s/m)	2.0×10^5
Damping coefficient at crane d_0 (N m s/rad)	8.0×10^5
Seawater density ρ_s (kg m ⁻³)	1024

to test the robustness of the controller. The sensor delay τ is considered as 0.1 s. Note that $q_1 = q_2 = \sqrt{\frac{T_0}{\rho}}$, $c_1 = c_2 = \frac{d_c}{2\rho}$. p, q satisfy [Assumption 1](#) ($|pq| = 1 < e^{\frac{c_2}{q_2} + \frac{c_1}{q_1}} = 1.0014$), and

$$A_0 = \frac{-d_0}{M_0} - \frac{\sqrt{T_0\rho}}{M_0}, \quad E_0 = \frac{\sqrt{T_0\rho}}{M_0}, \quad B_0 = \frac{1}{M_0}, \quad C_0 = 2, \quad (187)$$

$$A_1 = \frac{-d_L}{M_L} + \frac{\sqrt{T_0\rho}}{M_L}, \quad B_1 = -\frac{\sqrt{T_0\rho}}{M_L}, \quad C_1 = 2 \quad (188)$$

satisfy [Assumptions 2–4](#). Ocean current disturbances $f(x, t), f_L(t)$ are modeled in Sec. 6.1.3 in [Wang and Krstic \(2019b\)](#).

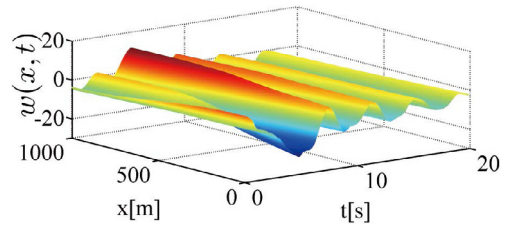
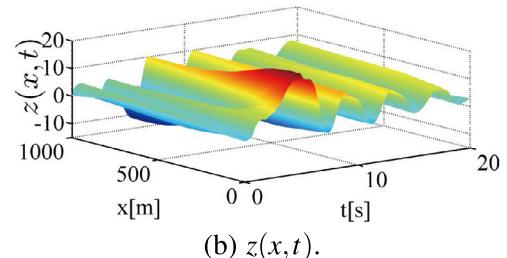
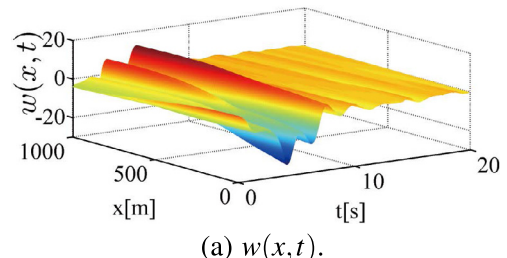
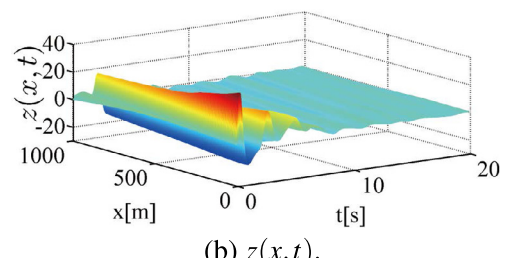
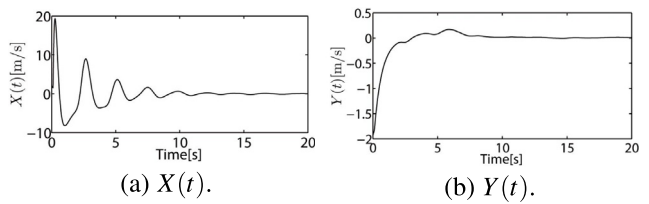
The initial conditions are defined as $z(x, 0) = 4 \sin(\frac{\pi x}{L})$, $w(x, 0) = 4 \cos(\frac{\pi x}{L})$, thereby, $X(0) = 2$, $Y(0) = -2$ recalling (181), (184) which physically mean initial oscillation velocities of the crane and payload. The initial oscillation velocity of the cable $u_t(x, 0)$ can be known based on the initial conditions of (180)–(186), i.e., $z(x, 0), w(x, 0)$, as $u_t(x, 0) = \frac{1}{2}(z(x, 0) + w(x, 0)) = 2 \sin(\frac{\pi x}{L}) + 2 \cos(\frac{\pi x}{L})$. The initial distributed oscillation displacement of the cable is defined as $u(x, 0) = 0$, thereby, initial offset of the payload $b_L(0) = 0$, and $b_0(0) = 0$ according to (213), (215) in [Wang and Krstic \(2019b\)](#).

6.2. Simulation results

Our task is to reduce the oscillations of cable and place the payload in the target area, namely within the permissible tolerance 2.5 m around the predetermined location ([How et al., 2011](#)), by applying the observer-based output-feedback control force at the onboard crane. We consider the end phase (20 s) of the descending process, i.e., the payload near the seafloor and the cable being the total length L , which is the most important and challenging phase because the cable is long and the oscillations would be large. The simulation is based on (180)–(186) using the finite difference method with the time step and the space step as 0.001 s and 0.1 m respectively. Considering the sensor delay $\tau = 0.1$ s, the measurement output is the 100-time-steps-earlier one. Applying the proposed designs into building the observer and controller for DCV (180)–(188), of which details are shown in Sec. 6.2 in [Wang and Krstic \(2019b\)](#), the following simulation results are observed.

6.2.1. Responses of z, w, X, Y

According to [Fig. 4](#), we know the oscillations appear in the responses of $w(x, t), z(x, t)$, which is the result of the property of the long cable and the external disturbances (230)–(231) in [Wang and Krstic \(2019b\)](#). From [Fig. 5](#), we can observe that the designed control input can effectively reduce the oscillation amplitudes even though the plant is subject to the external disturbances. The moving velocity of the controlled crane and the oscillation

(a) $w(x, t)$.(b) $z(x, t)$.**Fig. 4.** Responses of $w(x, t), z(x, t)$ (without control).(a) $w(x, t)$.(b) $z(x, t)$.**Fig. 5.** Responses of $w(x, t), z(x, t)$ (with control).(a) $X(t)$.(b) $Y(t)$.**Fig. 6.** Responses of $X(t), Y(t)$ (with control).

velocity of the payload, namely $X(t)$ and $Y(t)$, are shown in [Fig. 6](#) from which we know $X(t)$ and $Y(t)$ are convergent to zero. It also can be seen in [Fig. 7](#) that the observer errors $\tilde{w}(x, t), \tilde{z}(x, t)$ converge to a small range around zero under the unknown external disturbances and the sensor delay τ .

6.2.2. Representing the obtained responses as u, b_L in DSV

The physical meaning of the responses z, w in [Figs. 5–6](#) would be clear after representing them as the responses of the cable oscillation and position error, i.e., u and b_L in (212)–(216)

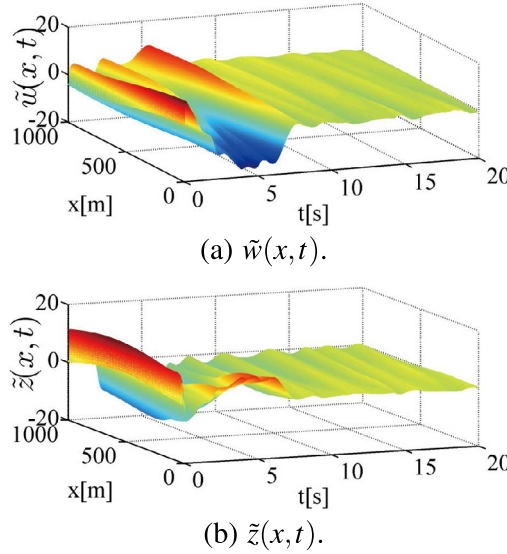


Fig. 7. Observer errors $\tilde{w}(x, t)$, $\tilde{z}(x, t)$.

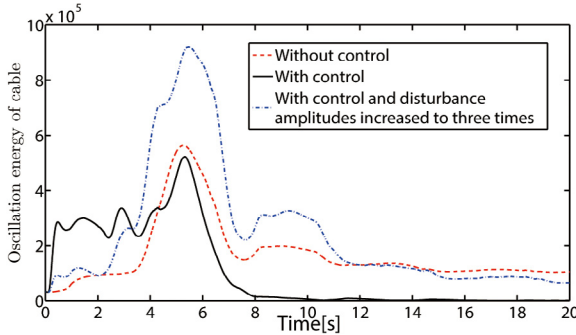


Fig. 8. Cable transverse oscillation energy: $\frac{\rho}{2} \|u_t(\cdot, t)\|^2 + \frac{T_0}{2} \|u_x(\cdot, t)\|^2$.

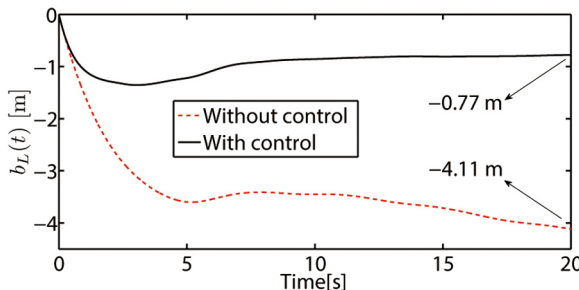


Fig. 9. Transverse displacement $b_L(t)$ of the payload. The end point at $t = 20$ s means the position error on the sea floor. The permissible tolerance of this typical model is 2.5 m (How et al., 2011).

of Wang and Krstic (2019b). Through (178)–(179), the cable transverse oscillation energy including oscillation kinetic energy $\frac{\rho}{2} \|u_t(\cdot, t)\|^2$ and potential energy $\frac{T_0}{2} \|u_x(\cdot, t)\|^2$ can be represented by $z(x, t)$, $w(x, t)$ as $\frac{\rho}{2} \|u_t(\cdot, t)\|^2 + \frac{T_0}{2} \|u_x(\cdot, t)\|^2 = \frac{\rho}{8} \|w(\cdot, t) + z(\cdot, t)\|^2 + \frac{\rho}{8} \|w(\cdot, t) - z(\cdot, t)\|^2$, where $\|u_t(\cdot, t)\|^2$ denotes $\int_0^L u_t(\cdot, t)^2 dx$. The transverse displacement of the payload $b_L(t)$ can be obtained as $b_L(t) = u(L, t) = \frac{1}{2} \int_0^L (z(L, \delta) + w(L, \delta)) d\delta + b_L(0)$.

As shown in Fig. 8, the oscillation energy of the cable with the proposed control law is reduced faster and to a level below to the uncontrolled case after $t = 5.5$ s, under the external disturbances (230)–(231) in Wang and Krstic (2019b). This result

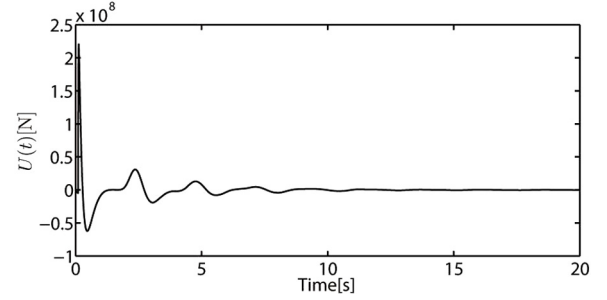


Fig. 10. Control force of the onboard crane.

shows robustness of the proposed control to small disturbances. However, as we continue to increase the amplitude of the disturbance (230) in Wang and Krstic (2019b) by gradually raising A_D i.e., the amplitude of the oscillating drag force, from its baseline value 400, the blue line in Fig. 8 shows that the controller fails to achieve effective vibration suppression once A_D reaches three times the baseline value, i.e., $A_D = 1200$. From Fig. 9, we note that the position error of the payload is -0.77 m from the desired location on the sea floor, which satisfies the requirement of being within permissible tolerance of 2.5 m, while the position error is -4.11 m in the case without control, which exceeds the tolerance. The control force shown in Fig. 10, is bounded and convergent.

7. Conclusion and future work

Delay-compensated control of heterodirectional coupled hyperbolic PDEs sandwiched between two general ODEs is addressed in this paper, where the control input is applied at one ODE and the measurement is placed at another ODE with a sensor delay. Using the delayed measurement output, a full-order state observer which can compensate the sensor delay is designed to estimate the states of the overall system including the plant and sensor delay dynamics. An observer-based output-feedback controller is designed using backstepping transformations and frequency-domain design methods. The exponential stability result of the closed-loop system and the boundedness and exponential convergence of the control input are proved in this paper. The obtained theoretical results are applied to oscillation suppression of a DCV for off-shore oil drilling as a simulation case. The simulation results show the proposed control input applied at the onboard crane can reduce the oscillations of the cable and place the payload in the target area on the sea floor.

In this paper, the observer-based output-feedback controller is designed based on the model with completely known parameters. In the future work, the model uncertainties, such as unknown plant parameters and external disturbances will be considered in such a sandwiched PDE system, and the adaptive and ADRC (Active Disturbance Rejection Control) technologies would be incorporated into the control design to solve this more practical and complex problem including parameter estimation and disturbance attenuation.

References

- Ahmed-Ali, T., Karafyllis, I., & Laminabhi-Lagarrigue, F. (2013). Global exponential sampled-data observers for nonlinear systems with delayed measurements. *Systems & Control Letters*, 62, 539–549.
- Anfinsen, H., & Aamo, O. M. (2017). Disturbance rejection in general heterodirectional 1-D linear hyperbolic systems using collocated sensing and control. *Automatica*, 76, 230–242.
- Anfinsen, H., & Aamo, O. M. (2018). Stabilization of a linear hyperbolic PDE with actuator and sensor dynamics. *Automatica*, 95, 104–111.

Basturk, H. I., & Krstic, M. (2014). State derivative feedback for adaptive cancellation of unmatched disturbances in unknown strict-feedback LTI systems. *Automatica*, 50, 2539–2545.

Bin, M., & Di Meglio, F. (2016). Boundary estimation of boundary parameters for linear hyperbolic PDEs. *IEEE Transactions on Automatic Control*, 62(8), 3890–3904.

Bou Saba, D., Bribiesca Argomedo, F., Di Loreto, M., & Eberard, D. (2017). Backstepping stabilization of 2×2 linear hyperbolic PDEs coupled with potentially unstable actuator and load dynamics. In *56th IEEE conference on decision and control (CDC)* (pp. 2498–2503).

Bou Saba, D., Bribiesca-Argomedo, F., Loreto, M. D., & Eberard, D. (2019). Strictly Proper Control Design for the stabilization of 2×2 Linear Hyperbolic ODE-PDE-ODE systems. In *58th IEEE conference on decision and control (CDC)* (pp. 4996–5001).

Cacace, F., Germani, A., & Manes, C. (2010). An observer for a class of nonlinear systems with time varying observation delay. *Systems & Control Letters*, 59(5), 305–312.

Deutscher, J. (2017a). Finite-time output regulation for linear 2×2 hyperbolic systems using backstepping. *Automatica*, 75, 54–62.

Deutscher, J. (2017b). Output regulation for general linear heterodirectional hyperbolic systems with spatially-varying coefficients. *Automatica*, 85, 34–42.

Deutscher, J., Gehring, N., & Kern, R. (2018). Output feedback control of general linear heterodirectional hyperbolic ODE-PDE-ODE systems. *Automatica*, 95, 472–480.

Deutscher, J., Gehring, N., & Kern, R. (2019). Output feedback control of general linear heterodirectional hyperbolic PDE-ODE systems with spatially-varying coefficients. *International Journal of Control*, 92, 2274–2290.

Di Meglio, F., Bribiesca, F., Hu, L., & Krstic, M. (2018). Stabilization of coupled linear heterodirectional hyperbolic PDE-ODE systems. *Automatica*, 87, 281–289.

Di Meglio, F., Lamare, P.-O., & Aarsnes, Ulf Jakob F. (2020). Robust output feedback stabilization of an ODE-PDE-ODE interconnection. *Automatica*, 119, 109059.

Germani, A., Manes, C., & Pepe, P. (2002). A new approach to state observation of nonlinear systems with delayed output. *IEEE Transactions on Automatic Control*, 47(1), 96–101.

Guerrero, M. E., Mercado, D. A., Lozano, R., & Garcia, C. D. (2015). Passivity based control for a quadrotor UAV transporting a cable-suspended payload with minimum swing. In *IEEE 54th annual conference on decision and control*.

Guo, B.-Z., & Xu, C.-Z. (2008). Boundary output feedback stabilization of a one-dimensional wave equation system with time delay. *IFAC Proceedings of Volumes*, 41(2), 8755–8760.

He, W., & Ge, S. S. (2012). Robust adaptive boundary control of a vibrating string under unknown time-varying disturbance. *IEEE Transactions on Control Systems Technology*, 20, 48–58.

He, W., & Ge, S. S. (2016). Cooperative control of a nonuniform gantry crane with constrained tension. *Automatica*, 66, 146–154.

He, X., He, W., Shi, J., & Sun, C. (2017). Boundary vibration control of variable length crane systems in two-Dimensional space with output constraints. *IEEE/ASME Transactions on Mechatronics*, 22(5), 1952–1962.

He, W., Meng, T., He, X., & Ge, S. S. (2018). Unified iterative learning control for flexible structures with input constraints. *Automatica*, 96, 326–336.

How, B., Ge, S. S., & Choo, Y. S. (2010). Dynamic load positioning for subsea installation via adaptive neural control. *IEEE Journal of Oceanic Engineering*, 35, 366–375.

How, B., Ge, S. S., & Choo, Y. S. (2011). Control of coupled vessel, crane, cable, and payload dynamics for subsea installation operations. *IEEE Transactions on Control Systems Technology*, 19, 208–220.

Krstic, M. (2008). Lyapunov tools for predictor feedbacks for delay systems: Inverse optimality and robustness to delay mismatch. *Automatica*, 44(11), 2930–2935.

Krstic, M. (2009). *Delay compensation for nonlinear, adaptive, and PDE systems*. Springer.

Krstic, M. (2010a). Compensation of infinite-dimensional actuator and sensor dynamics: Nonlinear and delay-adaptive systems. *IEEE Control Systems Magazine*, 30, 22–41.

Krstic, M. (2010b). Lyapunov stability of linear predictor feedback for timevarying input delay. *IEEE Transactions on Automatic Control*, 55(2), 554–559.

Krstic, M., & Smyshlyaev, A. (2008). Backstepping boundary control for first-order hyperbolic PDEs and application to systems with actuator and sensor delays. *Systems & Control Letters*, 57(9), 750–758.

Liu, W.-J., & Krstic, M. (2000). Backstepping boundary control of Burgers' equation with actuator dynamics. *Systems & Control Letters*, 41, 291–303.

Moylan, P. J. (1977). Stable inversion of linear systems. *IEEE Transactions on Automatic Control*, 74–78.

Palunko, I., Cruz, P., & Fierro, R. (2012). Agile load transportation: Safe and efficient load manipulation with aerial robots. *IEEE Robotics & Automation Magazine*, 19(3), 69–79.

Sharma, R. (2017). *Deep-sea mining*. Springer.

Standing, R. G., Mackenzie, B. G., & Snell, R. O. (2002). Enhancing the technology for deepwater installation of subsea hardware. In *Offshore technology conference*.

Stensgaard, T., White, C., & Schiffer, K. (2010). Subsea hardware installation from a FDPSO. In *Offshore technology conference*.

Wang, J., Koga, S., Pi, Y., & Krstic, M. (2018). Axial vibration suppression in a PDE Model of ascending mining cable elevator. *Journal of Dynamic Systems, Measurement, and Control*, 140, Article 111003.

Wang, J., & Krstic, M. (2019a). Output-feedback boundary control of a heat PDE sandwiched between two ODEs. *IEEE Transactions on Automatic Control*, 64(11), 4653–4660.

Wang, J., & Krstic, M. (2019b). (Supplementary document) Delay-compensated control of sandwiched ODE-PDE-ODE hyperbolic systems for oil drilling and disaster relief. arXiv preprint [arXiv:1910.05948](https://arxiv.org/abs/1910.05948).

Wang, J., & Krstic, M. (2020). Vibration suppression for coupled wave PDEs in deep-sea construction. in press.

Wang, J., Krstic, M., & Pi, Y. (2018). Control of a 2×2 coupled linear hyperbolic system sandwiched between two ODEs. *International Journal of Robust and Nonlinear Control*, 28, 3987–4016.

Wang, J., Pi, Y., Hu, Y.-M., & Zhu, Z.-C. (2020). State-observer design of a PDE-modeled mining cable elevator with time-varying sensor delays. *IEEE Transactions on Control Systems Technology*, 28(3), 1149–1157.

Wang, J., Pi, Y., & Krstic, M. (2018). Balancing and suppression of oscillations of tension and cage in dual-cable mining elevators. *Automatica*, 98, 223–238.

Willmann, J., Augugliaro, F., Cadalbert, T., D'Andrea, R., Gramazio, F., & Kohler, M. (2012). Aerial robotic construction towards a new field of architectural research. *International Journal of Architectural Computing*, 10(3), 439–459.



Ji Wang received the Ph.D. degree in Mechanical Engineering in 2018 from Chongqing University, Chongqing, China. He is currently a Postdoctoral Scholar-Employee in the Department of Mechanical and Aerospace Engineering at University of California, San Diego, La Jolla, CA, USA. His research interests include modeling and control of distributed parameter systems with applications in control of string-actuated motion.



Miroslav Krstic is Distinguished Professor of Mechanical and Aerospace Engineering, holds the Alspach endowed chair, and is the founding director of the Cymer Center for Control Systems and Dynamics at UC San Diego. He also serves as Senior Associate Vice Chancellor for Research at UCSD. As a graduate student, Krstic won the UC Santa Barbara best dissertation award and student best paper awards at CDC and ACC. Krstic has been elected Fellow of seven scientific societies – IEEE, IFAC, ASME, SIAM, AAAS, IET (UK), and AIAA (Assoc. Fellow) – and as a foreign member of the

Serbian Academy of Sciences and Arts and of the Academy of Engineering of Serbia. He has received the SIAM Reid Prize, ASME Oldenburger Medal, Nyquist Lecture Prize, Paynter Outstanding Investigator Award, Ragazzini Education Award, IFAC Nonlinear Control Systems Award, Chestnut textbook prize, Control Systems Society Distinguished Member Award, the PECASE, NSF CAREER, and ONR Young Investigator awards, the Schuck ('96 and '19) and Axelby paper prizes, and the first UCSD Research Award given to an engineer. Krstic has also been awarded the Springer Visiting Professorship at UC Berkeley, the Distinguished Visiting Fellowship of the Royal Academy of Engineering, and the Invitation Fellowship of the Japan Society for the Promotion of Science. He serves as Editor-in-Chief of *Systems & Control Letters* and has been serving as Senior Editor in *Automatica* and *IEEE Transactions on Automatic Control*, as editor of two Springer book series, and has served as Vice President for Technical Activities of the IEEE Control Systems Society and as chair of the IEEE CSS Fellow Committee. Krstic has coauthored thirteen books on adaptive, nonlinear, and stochastic control, extremum seeking, control of PDE systems including turbulent flows, and control of delay systems.